Probab. Theory Relat. Fields (2015) 162:275–325
DOI 10.1007/s00440-014-0573-9

Tacnode GUE-minor processes and double Aztec diamonds

Mark Adler · Sunil Chhita · Kurt Johansson · Pierre van Moerbeke

Received: 2 April 2013 / Revised: 23 May 2014 / Published online: 25 July 2014

Abstract We study determinantal point processes arising in random domino tilings of a double Aztec diamond, a region consisting of two overlapping Aztec diamonds. At a turning point in a single Aztec diamond where the disordered region touches the boundary, the natural limiting process is the GUE-minor process. Increasing the size of a double Aztec diamond while keeping the overlap between the two Aztec diamonds finite, we obtain a new determinantal point process which we call the tacnode GUE-minor process. This process can be thought of as two colliding GUE-minor processes.

The support of a National Science Foundation Grant # DMS-07-00782 and Simons Foundation Grant National Science Foundation Grant # 278931 is gratefully acknowledged by M. Adler.
The support of the Knut and Alice Wallenberg Foundation Grant KAW 2010.0063 is gratefully acknowledged by S. Chhita.

The support of the Swedish Research Council (VR) and grant KAW 2010.0063 of the Knut and Alice Wallenberg Foundation are gratefully acknowledged by K. Johansson.
The support of a National Science Foundation Grant # DMS-07-00782, FNRS and Simons Foundation Grant National Science Foundation Grant # 280945 is gratefully acknowledged by P. van Moerbeke.

M. Adler · P. van Moerbeke
Department of Mathematics, Brandeis University, Waltham, MA 02454, USA
e-mail: adler@brandeis.edu

S. Chhita (✉)
Institute of Applied Mathematics, University of Bonn, Bonn, Germany
e-mail: chhita@kth.se

K. Johansson
Department of Mathematics, Royal Institute of Technology (KTH), Stockholm, Sweden
e-mail: kurtj@kth.se

P. van Moerbeke
Department of Mathematics, Université de Louvain, 1348 Louvain-la-Neuve, Belgium
e-mail: pierre.vanmoerbeke@UCLouvain.be; vanmoerbeke@brandeis.edu

As part of the derivation of the particle kernel whose scaling limit naturally gives the tacnode GUE-minor process, we find the inverse Kasteleyn matrix for the dimer model version of the Double Aztec diamond.

Keywords Interlacing · Random tiling · Kasteleyn · Dimer · Airy process · Extended kernels · Random Hermitian ensembles

Mathematics Subject Classification (2010) Primary 60G60 · 60G65 · 35Q53; Secondary 60G10 · 35Q58

Contents

1 Introduction and main results . . . 276
1.1 Domino tilings of double Aztec diamonds and random surface . . . 279
1.2 Two determinantal point processes $\mathbb{L}$ and $\mathbb{K}$ . . . 283
1.2.1 The $\mathbb{L}$-process . . . 283
1.2.2 The $\mathbb{K}$-process . . . 285
1.3 The Tacnode GUE-minor kernel and the main theorem . . . 287
2 The kernel for the $\mathbb{L}$-process, via Kasteleyn . . . 290
2.1 The $\mathbb{L}$-particle process . . . 290
2.2 The Kasteleyn matrix . . . 292
3 The tacnode GUE-minor kernel and its symmetry . . . 295
4 Interlacing pattern of the $\mathbb{L}$-process . . . 297
5 Scaling limit of the $\mathbb{L}$ and $\mathbb{K}$-processes . . . 300
6 Proof of the inverse Kasteleyn formula . . . 308
6.1 The interior . . . 310
6.2 The left hand boundary . . . 313
6.3 The bottom boundary . . . 315
6.4 The top boundary . . . 317
6.5 The special point . . . 319
7 Proof of the formula for the $\mathbb{L}$-kernel . . . 320
References . . . 324

1 Introduction and main results

An Aztec diamond of order n consists of all squares of the square lattice whose centers (x, y) satisfy $|x| + |y| \leq n$ for $n \in \mathbb{N}$. A domino is a union of two adjacent squares. A domino tiling of an Aztec diamond, introduced in [8,9], is an arrangement of dominos such that each square of the Aztec diamond is covered exactly once by a domino. By assigning a weight to each domino, a domino tiling is picked at random with probability proportional to the product of the domino weights of the domino tiling. There are in fact four different types of dominos in a tiling: the dominos can be placed in two orientations, each of which comes in two different parities. These parities can be seen by giving the Aztec diamond a checkerboard coloring—for horizontal dominos, either the left square is black or it is white. Uniformly random tilings of large Aztec diamonds exhibit striking features—the main one being that these tilings exhibit a limit shape, described by the Arctic circle theorem [13]: for Aztec diamonds with high order and with asymptotically high probability there is an inscribed circle containing a disordered region which contains all four types of dominos while outside

this circle there are four frozen regions each containing one type of domino arranged in a regular brick wall pattern; see [10,14,15,23]. When the weight a of vertical dominos is different from the one of horizontal dominos, then the arctic circle gets replaced by an inscribed arctic ellipse.

In [2], the authors investigate the domino tiling of two overlapping Aztec diamonds, each of size n, with weight $0 < a < 1$ for vertical dominos and weight 1 for horizontal dominos. When the size of the diamonds and the overlap both become very large, in such a way that the two arctic ellipses for the single Aztec diamonds merely touch, then a new critical process, the *tacnode process*, will appear near the point of osculation (tacnode); it is run with a time in the direction of the common tangent to the ellipses. The kernel governing the local statistics of the tacnode process is given by a perturbation of the *Airy process kernel* by an integral of two functions. It was also shown in [2] that this tacnode process has some universal character: it coincides with the one found in the context of two groups of non-intersecting random walks [1] and Brownian motions, meeting momentarily [11,16]; see also [7].

Another ingredient here is the process given by the successive interlacing eigenvalues of minors of a GUE-matrix: the so-called GUE-minor process. In [17] this process has arisen in the following model: magnifying the infinitesimal region about the point of tangency of the arctic ellipses with the edge of a single Aztec diamond for large n, leads to a determinantal process of interlacing points on the successive lines through (say) the black squares, parallel to the edge of the diamond. This yields the GUE-minor process, see also [21].

In the present work, we consider two overlapping Aztec diamonds with an overlap, which remains finite, when the size of the diamonds tends to infinity. In order to maintain the osculation of the two inscribed ellipses, the geometry forces the weight a of the vertical dominos to tend to the weight of the horizontal dominos, say at rate $\beta\sqrt{2/n}$. Macroscopically this amounts to two Aztec diamonds with inscribed arctic circles intersecting infinitesimally. The top figure in Fig. 1 shows a relatively large simulation of a double Aztec diamond. In view of the comments above, it seems natural that this process be related to the GUE-minor kernel. Indeed, when n tends to infinity, looking with a magnifying glass at the infinitesimal overlap of the diamonds gives rise to a new determinantal point process, with local statistics given by the so-called *tacnode GUE-minor kernel*; it is a finite rank perturbation of the GUE-minor kernel mentioned above; see Theorems 1.4 and 1.5 in Sect. 1.3. The random matrix theory counterpart of this distribution, as described in [3], involves two GUE-matrices coupled together via the spectra of principal minors.

In [2], the authors considered successive lines through black squares perpendicular to the region of overlap with dots in the black square each time the dominos covering that square is pointing to the right of or above the line (green and red dominos, i.e., south and west as in Fig. 5); these are called the $\mathbb{K}$-particles. In this work, we shall mainly consider successive lines parallel to the region of overlap and put a dot in the black square each time the dominos covering that square is pointing to the right of or below that line (green and blue dominos, i.e., south and east as in Fig. 5); these give the $\mathbb{L}$-particles (Sect. 1.2). Figure 2 shows the $\mathbb{K}$ and $\mathbb{L}$-particles for the simulation drawn in Fig. 1.

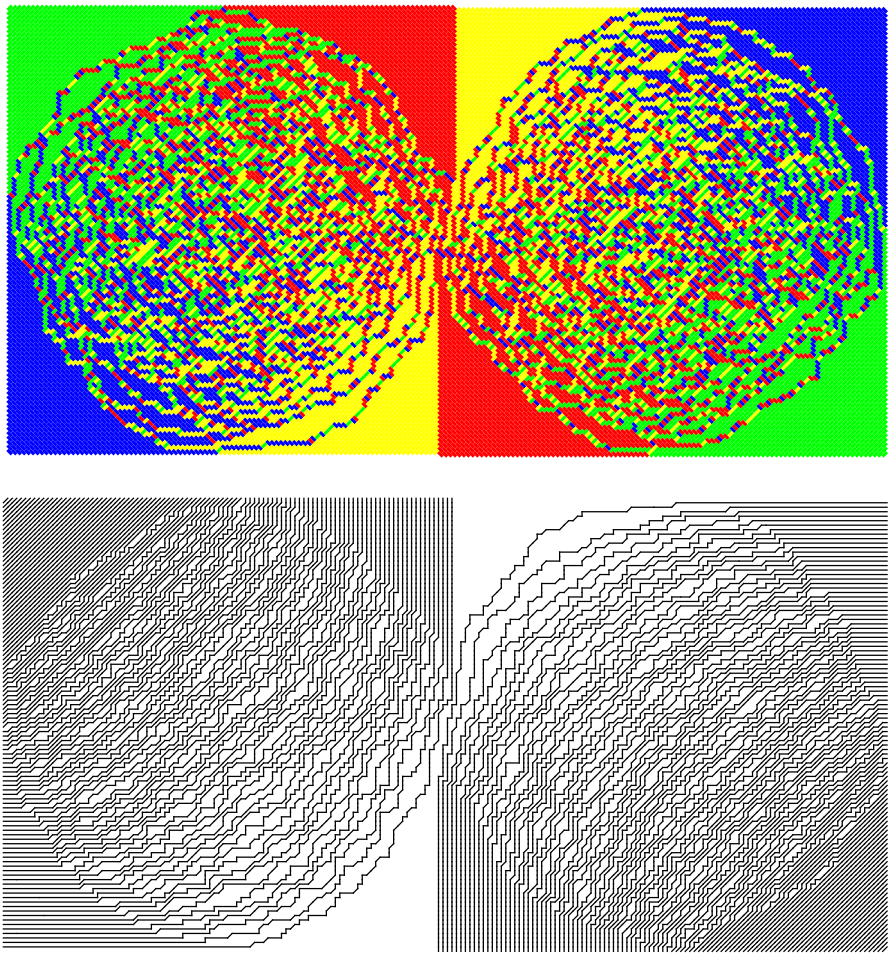

Fig. 1 A simulation of a double Aztec diamond with $n = 100$ and $\rho = 4$ with the weight a of vertical and horizontal tiles equal to 1. Both figures are rotated by $\pi/4$ counter-clockwise. The *top figure* shows the domino tiling with *four colors* representing the four types of dominos. The *bottom figure* shows the level lines of the height function for the tiling which are defined in Sect. 1.1. The simulation was made using the generalized domino shuffle [22] (color figure online)

In Theorem 1.1, we deduce the kernel for the $\mathbb{L}$-particles from the one of the $\mathbb{K}$-particles, by first obtaining in Theorem 2.3 (Sect. 6) the inverse Kasteleyn matrix [18] for the double Aztec diamond in terms of the $\mathbb{K}$-kernel and then deduce in Sect. 7 the $\mathbb{L}$-kernel of the particles from that same inverse Kasteleyn matrix. The inverse Kasteleyn matrix of a single Aztec diamond had been obtained for $a = 1$ by [12] and generalized for all a recently in [5]. A similar extension, that is using the Kasteleyn approach to go between two particle kernels has been used previously for lozenge tilings [4].

In Proposition 1.3, Sect. 1.2, we study the specific interlacing pattern of the $\mathbb{L}$-particles. We state in Theorem 1.4, Sect. 1.3 and prove in Sect. 5 that, in the scaling limit $n \to \infty$, the $\mathbb{L}$-process in the infinitesimal overlap is indeed driven by the

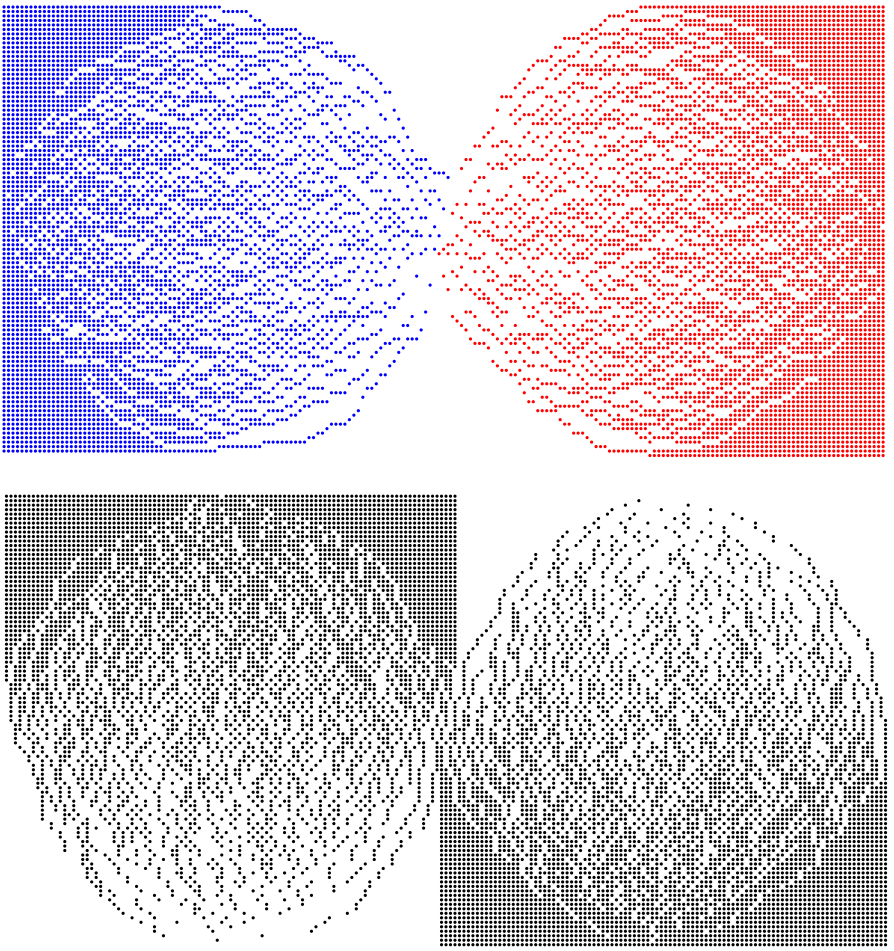

Fig. 2 The *top picture* shows the *blue* and *red* $\mathbb{L}$-particles for the simulation in Fig. 1. Roughly speaking, the $\mathbb{L}$-particles represent the *green* and *blue* dominos in both Aztec diamonds and are *colored* either *blue* or *red* depending on their location within the double Aztec diamond, see Sect. 1.2.1 for a complete description. The *bottom picture* shows the $\mathbb{K}$-particles for the same simulation in Fig. 1. The $\mathbb{K}$-particles represent the *red* and *green* dominos, see Sect. 1.2.2 for a complete description. *Both figures* have the same orientation as Fig. 1 (color figure online)

tacnode GUE-minor kernel. Also, we state in Theorem 1.5, Sect. 1.3 and prove in Sect. 5 that upon thinning at the rate $p_n = 1 - 2\sqrt{2/n}$, the $\mathbb{K}$-process is also driven by the same tacnode GUE-minor kernel, but with a (somewhat surprising) shift in one of the discrete parameters.

1.1 Domino tilings of double Aztec diamonds and random surface

Consider two overlapping Aztec diamonds A and B, of equal sizes n and overlap ρ, with opposite orientations; i.e., the upper-left square for diamond A is black and is

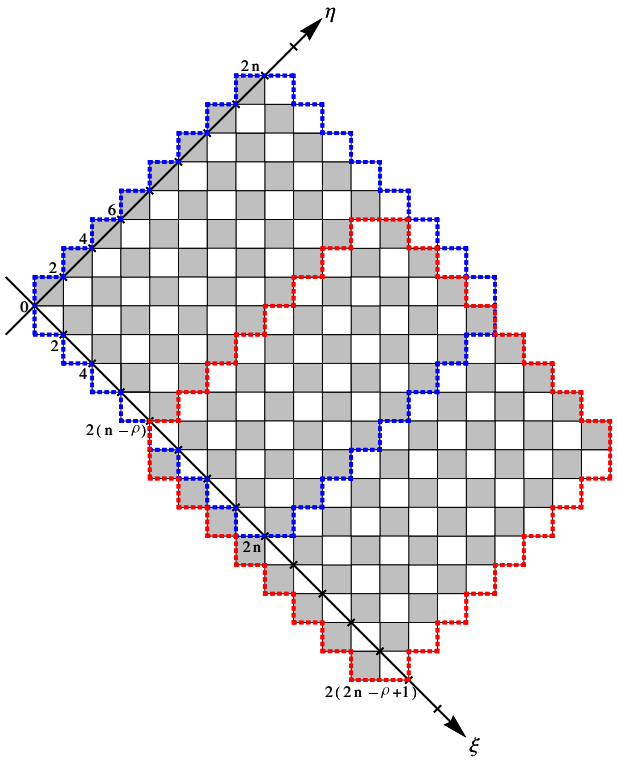

Fig. 3 Double Aztec diamond with $n = 8$ and overlap $\rho = 4$, with the (ξ, η) coordinates with Aztec diamond A enclosed by the *blue dotted line* and Aztec diamond B enclosed by the *red dotted line*. The overlap contains ρ lines (through *black squares*) $\xi = 2s$ for $n - \rho < s \leq n$ (color figure online)

white for diamond B. The size n is the number of squares on the upper-left side and the amount of overlap ρ counts the number of lines of black squares common to both diamonds A and B. Let ξ, η be a system of coordinates as indicated in Fig. 3. The even lines $\xi = 2k$ for $0 \leq k \leq 2n - \rho$ and the odd lines $\eta = 2k - 1$ for $1 \leq k \leq n$ run through black squares. The ρ even lines $\xi = 2(n - \rho + 1), \ldots, 2n$ belong to the overlap of the two diamonds. Dominos can be placed either vertically or horizontally on the double Aztec diamond. We pick a domino tiling T at random with probability proportional to $a^{v(T)}$, where $v(T)$ is the number of vertical dominos in T. We assign the terms North, South, East and West to each type of domino, as given in Fig. 4.

Define

$$M := n - \rho + 1 = \#\left\{\begin{array}{l}\text{white squares of diamond } A \text{ along the line } \eta = 0,\\ \text{having an edge in common with the boundary}\end{array}\right\},$$

and define m such that

$$M - 1 = n - \rho = \begin{cases} 2m & \text{when } n \text{ and } \rho \text{ have same parity} \\ 2m - 1 & \text{when } n \text{ and } \rho \text{ have opposite parity.} \end{cases}$$

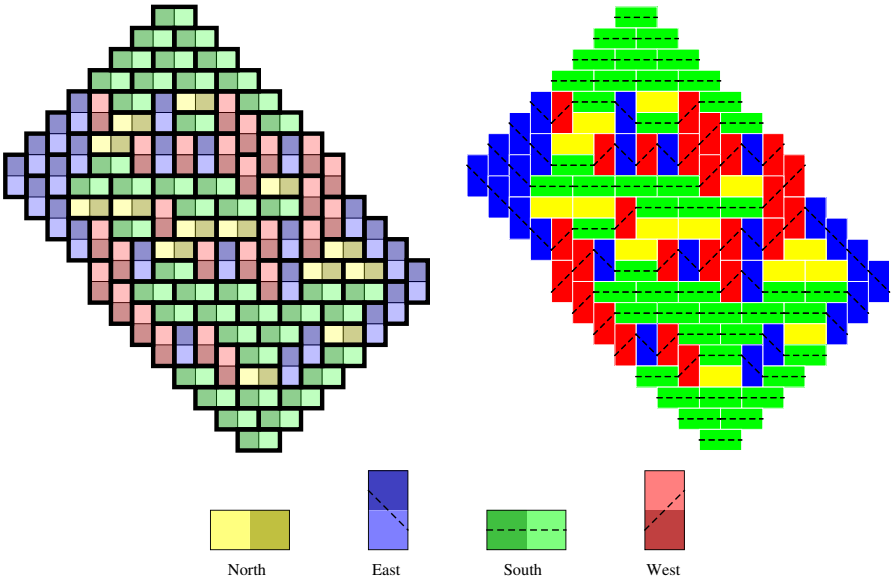

Fig. 4 Random tiling of a double Aztec diamond with $n = 8$ and $\rho = 4$. The *figure* on the *left* shows the underlying checkerboard structure while the *figure* on the *right* shows the same tiling with the level lines. These are shown explicitly for the four types of dominos in the *bottom figure*. These level lines are the same as the DR lattice paths [20]

Throughout the paper we assume, for simplicity, the same parity for n and ρ, so that $n - \rho = 2m$.

Together with this arbitrary domino-tiling of the double Aztec diamond $A \cup B$, one defines a piecewise-linear random surface, by means of a height function h specified by the heights, prescribed on the single dominos according to Fig. 5; this height can be taken to be piecewise-linear on each domino. This height function is different from the usual one by Cohn et al. [6], but related to it by an affine transformation. Let the upper-most edge of the double diamond $A \cup B$ have height $h = 0$. Then, regardless of the covering by dominos, the height function along the boundary of the double diamond will always be as indicated in Fig. 5, with height $h = 2n$ along the lower-most edge of the double diamond. Away from the boundary the height function will, of course, depend on the tiling; the associated heights are given in Fig. 5.

The height function h obtained in this way defines the domino tiling in a *unique* way, because a white square together with its height specifies in a unique way to which domino it belongs to: North, South, East and West; the same holds for black squares.

This height function associates thus a piece-wise linear random surface with each random tiling and two groups of level curves of this random surface corresponding to the half-integer values:

$$\underbrace{\frac{1}{2}, \frac{3}{2}, \frac{5}{2}, \ldots, n - \frac{1}{2}}_{A\text{-level curves}}, \quad \underbrace{n + \frac{1}{2}, \ldots, 2n - \frac{1}{2}}_{B\text{-level curves}}.$$

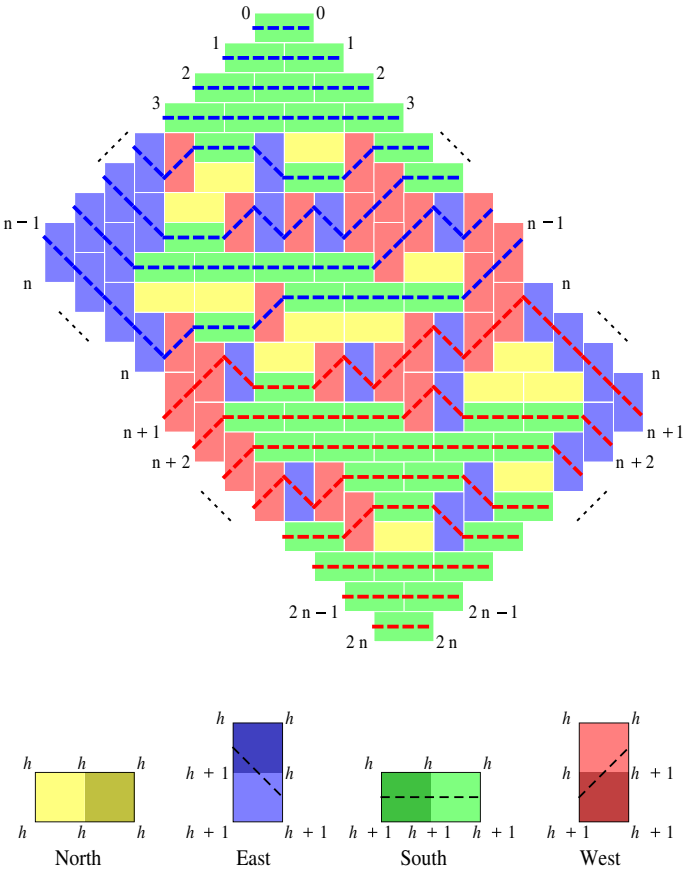

Fig. 5 The level lines including the height function around the boundary. The heights change in the interior only when crossing a level line. The *bottom figure* shows the height change for each individual domino

Put the weight $a > 0$ on vertical dominoes and the weight 1 on horizontal dominoes, so that the probability of a tiling configuration T can be expressed as

$$\mathbb{P}\,(\text{domino tiling } T) = \frac{a^{\#\text{vertical domino}'\text{s in}\,T}}{\sum_{\text{all possible tilings}\,T} a^{\#\text{vertical domino}'\text{s in}\,T}}$$

Remember $2m := n - \rho$ throughout the paper. We will also use the coordinates indicated in Fig. 6. These are the coordinates, which we will call diamond coordinates, that were used for the particle processes in [2]. The transformation from diamond coordinates (z, x) to Kasteleyn coordinates (ξ, η) is given by:

$$\begin{aligned} z &= \eta + 1 \\ x &= \tfrac{1}{2}(\eta - \xi + 2m + 1) \end{aligned} \iff \begin{aligned} \xi &= z - 2x + 2m \\ \eta &= z - 1 \end{aligned} \tag{1.1}$$

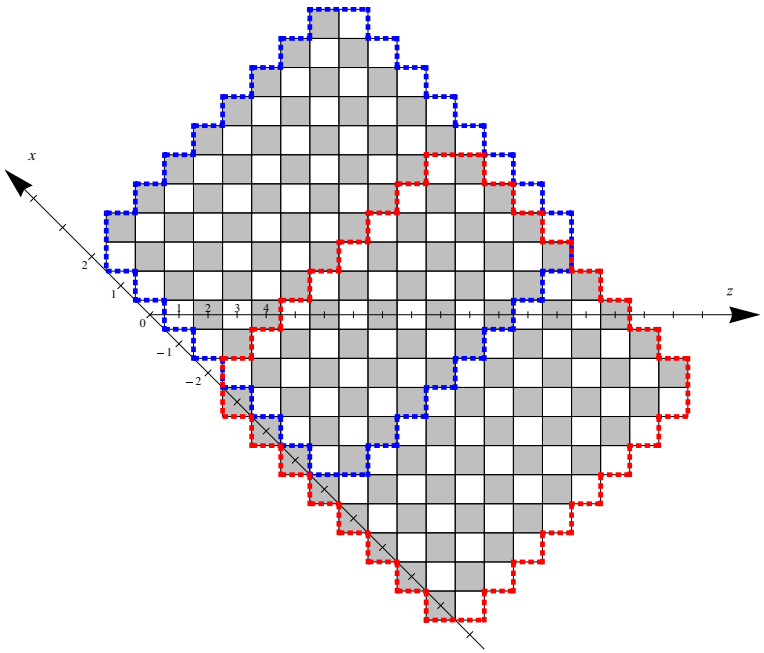

Fig. 6 Double Aztec diamond with $n = 8$ and overlap $\rho = 4$ with the (z, x) coordinates of the Aztec diamond

1.2 Two determinantal point processes $\mathbb{L}$ and $\mathbb{K}$

1.2.1 The $\mathbb{L}$-process

The $\mathbb{L}$ process is specified by putting a dot in the middle of the black square when the line $\xi = 2s$ in (ξ, η)-coordinates for $0 \le s \le 2n - \rho$ intersects a level curve. We call these dots $\mathbb{L}$-*particles*. See Fig. 7 for an example. More precisely we can put a blue dot when intersecting A-level curves and a red dot when intersecting B-level curves to distinguish the dots coming from the two Aztec diamonds; see Fig. 8. In other terms, put a dot in the black square each time the random surface goes down one unit along the line $\xi = 2s$.

We are concerned with the probabilities of the following kinds of events, where $[k, \ell]$ is an interval of odd integers along the η-axis (so k and ℓ can be taken odd):

$$
\begin{aligned}
&\{\text{The line } \{\xi = 2s\} \text{ has an } \eta\text{-gap} \supset [k, \ell]\}\\
&= \{\text{Interval } [k, \ell] \subset \{\xi = 2s\} \text{ in } \eta\text{-coordinates contains no dot-particles}\}\\
&= \{\text{The random surface is flat along the } \eta\text{-interval } [k, \ell] \subset \{\xi = 2s\}\}\\
&= \{\text{Dominos covering } [k, \ell] \subset \{\xi = 2s\} \text{ are pointing to the left of}\\
&\quad \text{or above the line } \{\xi = 2s\}\}\\
&= \{\text{Dominos covering } [k, \ell] \subset \{\xi = 2s\} \text{ are red or yellow in upper Fig. 7}\}
\end{aligned}
$$

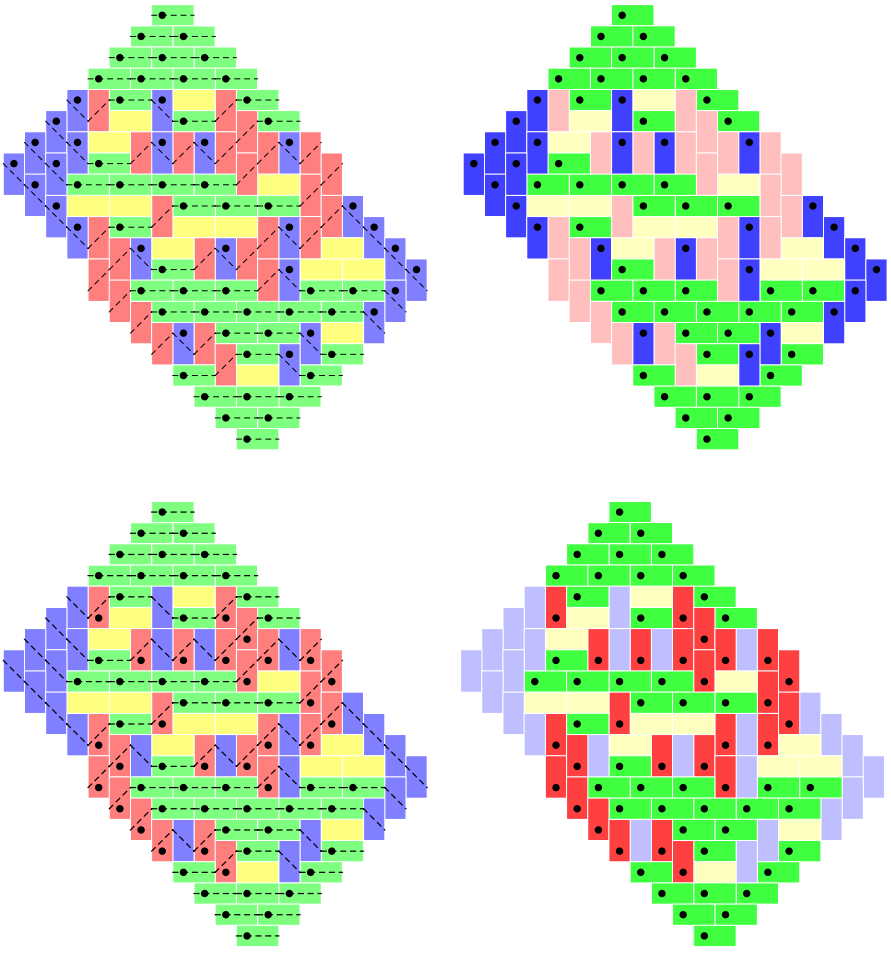

Fig. 7 The *top figures* show the $\mathbb{L}$ particle process using the level lines (on the *left*) and the dominos on the *right*. There is an $\mathbb{L}$ particle for every *green* (south) and blue (east) domino. The *bottom figures* show the $\mathbb{K}$ particle process. There is a $\mathbb{K}$ particle for every *green* (south) and *red* (west) domino (color figure online)

Theorem 1.1 *The $\mathbb{L}$-particles on the successive lines $\{\xi = 2s\}$ for $1 \le s \le 2n - \rho$ form a determinantal point process with correlation kernel*[1]

$$\mathbb{L}_{n,\rho}(\xi_1, \eta_1; \xi_2, \eta_2) = (1 + a^2)\mathbb{L}_n^{(0)}(\xi_1, \eta_1; \xi_2, \eta_2) - (1 + a^2)\langle((\mathbb{I} - K_n)^{-1}_{\ge n-\rho+1} A_{\xi_1,\eta_1})(.), B_{\xi_2,\eta_2}(.)\rangle_{\ge n-\rho+1}. \tag{1.2}$$

[1] $\langle f(.), g(.)\rangle_{\ge\alpha} = \sum_{\alpha}^{\infty} f(k)g(k)$ is an inner product in $\ell^2[\alpha, \infty]$, while $A_{\ge\alpha}$ refers to the operator A restricted to $\ell^2[\alpha, \infty)$.

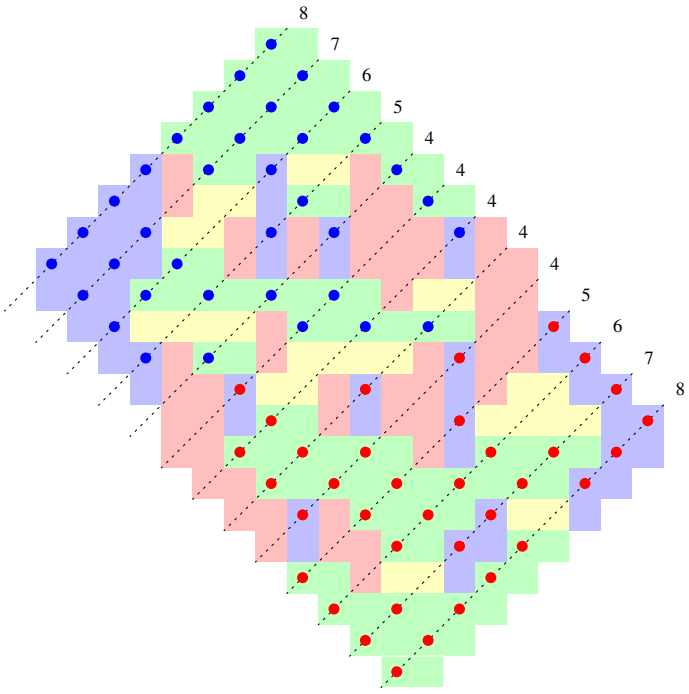

Fig. 8 The *red* and *blue* $\mathbb{L}$ particles. The *blue* $\mathbb{L}$ particles correspond to Aztec diamond A while the *red* particles correspond to Aztec diamond B see Fig. 3. The numbers represent the total number of particles on *each line* $\xi = 2s$ (color figure online)

given by a perturbation of a kernel $\mathbb{L}_n^{(0)}$ *by an inner-product involving the resolvent of yet another kernel* K_n*, all given by formulas* (2.2) (*Sect.* 2.1)*. This shows that, given* q *lines* $\{\xi = 2s_i\}$ *and integers* $k_i,\ \ell_i$*, with* $0 \le k_i < \ell_i \le n$*, the gap probability is expressed as the Fredholm determinant*[2]

$$\mathbb{P}\left(\bigcap_{i=1}^{q} \{\textit{The line } \{\xi = 2s_i\} \textit{ has an } \eta\textit{-gap} \supset [k_i, \ell_i]\}\right)$$
$$= \det\left(\mathbb{I} - \left[\chi_{[k_i,\ell_i]}(\eta_i)\mathbb{L}_{n,\rho}(2s_i, \eta_i; 2s_j, \eta_j)\chi_{[k_j,\ell_j]}(\eta_j)\right]_{1\le i,j\le q}\right),$$

of the kernel $\mathbb{L}_{n,\rho}$.

This theorem will be proved in Sect. 2.

1.2.2 The $\mathbb{K}$*-process*

Now we put instead a blue dot in the middle of the black square when the line $z = 2k$ in (z, x)-coordinates for $1 \le k \le n$ intersects an A-level curve and a red dot when

[2] The variables η_i below run through odd values only.

intersecting a B-level curve; i.e., put a dot each time the random surface goes down one unit along the line $z = 2k$; see Fig. 7. These dots define the $\mathbb{K}$-*particles*. In this instance, we are concerned with the probabilities of the following kinds of events, where $[k, \ell]$ is an interval along the x-axis:

$$\begin{aligned}
&\{\text{The line } \{z = 2r\} \text{ has an } x\text{-gap} \supset [k, \ell]\} \\
&\quad = \{\text{The interval } [k, \ell] \subset \{z = 2r\} \text{ in } x\text{-coordinates contains no dot-particles}\} \\
&\quad = \{\text{The random surface is flat along the } x\text{-interval } [k, \ell] \subset \{z = 2r\}\} \\
&\quad = \{\text{Dominos covering } [k, \ell] \subset \{z = 2r\} \text{ are pointing to the left or below } \{z = 2r\}\} \\
&\quad = \{\text{Dominos covering } [k, \ell] \subset \{z = 2r\} \text{ are blue or yellow in lower Fig. 7}\}
\end{aligned}$$

Theorem 1.2 ([2]) *The $\mathbb{K}$-particles on the successive lines $\{z = 2r\}$ for $1 \le r \le n$ form a determinantal point process with correlation kernel given by perturbing the one-Aztec diamond kernel $\mathbb{K}_n^0$ with an inner-product involving the resolvent of the kernel K_n, all defined in (2.4) and (2.5):*

$$\begin{aligned}
(-1)^{x-y}\mathbb{K}_{n,\rho}(2r, x; 2s, y) &= \mathbb{K}_n^0\big(2r, x; 2s, y\big) \\
&\quad - \Big\langle (\mathbb{I} - K_n)^{-1}_{\ge n-\rho+1} a_{-y,s}(.), b_{-x,r}(.) \Big\rangle_{\ge n-\rho+1}. \qquad (1.3)
\end{aligned}$$

This shows that given q lines $\{z = 2r_i\}$ and integers $k_i,\ \ell_i$, with $r_i - m - n \le k_i < \ell_i \le r_i + m$, we have

$$\begin{aligned}
&\mathbb{P}\left(\bigcap_{i=1}^{q} \{\text{the line } \{z = 2r_i\} \text{ has an } x\text{-gap} \supset [k_i, \ell_i]\}\right) \\
&\quad = \det\left(\mathbb{I} - \left[\chi_{[k_i,\ell_i]}(x_i)\mathbb{K}_{n,\rho}(2r_i, x_i; 2r_j, x_j)\chi_{[k_j,\ell_j]}(x_j)\right]_{1\le i,j\le q}\right).
\end{aligned}$$

with a kernel $\mathbb{K}_{n,\rho}$.

The theorem was proved in [2] where the $\mathbb{K}$-particles were called outlier particles.

The dot particles of the $\mathbb{L}$-process satisfy the following interlacing pattern.

Proposition 1.3 *For the $\mathbb{L}$-process, the lines $\xi = 2s$ contain blue dots and red dots, according to the following interlacing patterns, with varying numbers:*

lines $\xi = 2s$	*$\in$ Diamond*	*# of blue and red dots*
$0 \le s < n - \rho$	$\in A$	$n - s$ *blue dots*
$s = n - \rho$	$\in A$	ρ *blue dots*
$n - \rho < s < n$	$\in A \cap B$	ρ *dots with* { $n - s$ *blue dots*; *to the right of*; $s - n + \rho$ *red dots*; *for each* s }
$s = n$	$\in A \cap B$	ρ *red dots*
$n < s \le 2n - \rho$	$\in B$	$\rho + s - n$ *red dots*

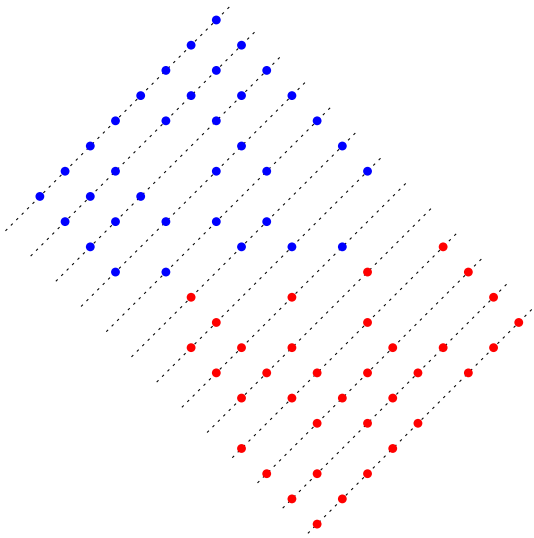

Fig. 9 The interlacing system of *blue* and *red dots*. The $\rho + 1$ lines, $\{\xi = 2s\} \in A \cap B$ and $\{\xi = 2(n - \rho)\} \in A$, contain ρ dots. All the other lines contain more dots. See Proposition 1.3 for more details on the interlacing (color figure online)

with interlacing of the blue dots and interlacing of the red dots, with regard to the η-coordinate; in the overlap of the two diamonds, the dots interlace as well, with the right most dot on the line $\xi = 2s$ being to the right of the right most dot on the line $\xi = 2s + 2$; also the left most dot on the line $\xi = 2s + 2$ is to the left of the left most dot on the line $\xi = 2s$. Notice that the overlap contains ρ lines (through black squares) $\xi = 2s$ with $n - \rho < s \leq n$. □

Figure 9 shows the above proposition schematically for the example tiling in Fig. 4. The proposition will be proved in Sect. 4.

It is interesting to notice that, passing from the $\mathbb{L}_{n,\rho}$-process to the $\mathbb{K}_{n,\rho}$-process, the dot is maintained in the horizontal dominos, whereas a dot in an East domino gets replaced by a dot in a West domino; compare the pictures given in Fig. 7.

Recall the $\mathbb{K}_{n,\rho}$-point process is a process of dots along the lines $\eta = 2k - 1$ or what is the same $z = 2k$. For the sake of the main theorem below, the point of view will be switched around: namely, the $\mathbb{K}_{n,\rho}$-process induces a determinantal process of dots along the lines $\xi = 0$ up to $\xi = 2(2n - \rho)$, inherited from the dots on the lines $z = 2k$. As mentioned, this process can be obtained from the $\mathbb{L}_{n,\rho}$-process by keeping the dots belonging to the horizontal domino's and moving the dots from the vertical domino's with a black square below to the vertical ones with a black square above; see Fig. 7.

1.3 The Tacnode GUE-minor kernel and the main theorem

For the rest of the paper, we denote $\Gamma_{a_1,a_2,\ldots,a_m}$ to be a positively oriented contour containing the points $a_1, \ldots, a_m$. Where convenient, we denote γ_r to be a positively oriented contour given by a circle of radius r containing the origin. We will also denote $L := 0^+ + i\mathbb{R}\uparrow$; the line L is situated to the right of the contour Γ_0.

The coupled GUE-minor kernel, depending on two parameters β, ρ, is defined to be:

$$\mathbb{K}^{\mathrm{tac}}_{\beta,\rho}(u_1, y_1; u_2, y_2) = \mathbb{K}^{\mathrm{minor}}(u_1, \beta - y_1;\ u_2, \beta - y_2) + 2\Big\langle (\mathbb{I} - \mathcal{K}^{\beta})^{-1}_{\geq -\rho}\, \mathcal{A}^{\beta, y_1-\beta}_{u_1}(.),\, \mathcal{B}^{\beta, y_2-\beta}_{u_2}(.)\Big\rangle_{\geq -\rho} \tag{1.4}$$

where $\mathbb{K}^{\mathrm{minor}}(n, x; n', x')$ is the GUE-minor kernel, defined for $n, n' \in \mathbb{Z}$, rather than $\mathbb{N}$. In the above equation, the subscript $\geq -\rho$ refers to the space $\ell^2(-\rho, \ldots, \infty)$. This kernel will appear below as the appropriate scaling limit of the $\mathbb{L}$-particle kernel. Define

$$\mathbb{K}^{\mathrm{minor}}(n, x; n', x') := -\mathbb{I}_{n>n'} 2^{n-n'} \mathbb{H}^{n-n'}(x - x') + \frac{2}{(2\pi \mathrm{i})^2} \int_{\Gamma_0} dz \int_{L} \frac{dw}{w - z} \frac{e^{-z^2+2zx}}{e^{-w^2+2wx'}} \frac{w^{n'}}{z^n},$$

with $\mathbb{H}^m(z)$ defined for $m \geq 1$ as

$$\mathbb{H}^m(z) := \tfrac{z^{m-1}}{(m-1)!} \mathbb{I}_{z\geq 0}.$$

The kernel defined in Eq. (1.4) contains the functions:

$$\begin{aligned}
\mathcal{K}^{\beta}(\lambda, \kappa) &:= \int_{\Gamma_0} \frac{d\zeta}{(2\pi \mathrm{i})^2} \int_{L} \frac{d\omega}{\omega - \zeta} \frac{e^{-2\zeta^2+4\beta\zeta}}{e^{-2\omega^2+4\beta\omega}} \frac{\zeta^{\kappa}}{\omega^{\lambda+1}} \\
\mathcal{A}^{\beta, y}_{v}(\kappa) &:= \int_{\Gamma_0} \frac{d\zeta}{(2\pi \mathrm{i})^2} \int_{L} \frac{d\omega}{\zeta - \omega} \frac{e^{-\zeta^2-2y\zeta}}{e^{-2\omega^2+4\beta\omega}} \frac{\zeta^{-v}}{\omega^{\kappa+1}} \int_{L} \frac{d\zeta}{2\pi \mathrm{i}} \frac{e^{\zeta^2-2\zeta(y+2\beta)}}{\zeta^{v+\kappa+1}} \\
\mathcal{B}^{\beta, y}_{u}(\lambda) &:= \int_{\Gamma_0} \frac{d\zeta}{(2\pi \mathrm{i})^2} \int_{L} \frac{d\omega}{\zeta - \omega} \frac{e^{-2\zeta^2+4\zeta\beta}}{e^{-\omega^2-2\omega y}} \frac{\zeta^{\lambda}}{\omega^{-u}} + \int_{\Gamma_0} \frac{d\omega}{2\pi \mathrm{i}} \frac{\omega^{u+\lambda}}{e^{\omega^2-2\omega(y+2\beta)}}.
\end{aligned} \tag{1.5}$$

To be precise in the limit theorems we should replace $\mathbb{I}_{z\geq 0}$ by $\mathbb{I}_{z>0} + \frac{1}{2}\mathbb{I}_{z=0}$ in the case of the $\mathbb{L}$-process, (1.7) in Theorem 1.4 below, and by $\mathbb{I}_{z>0}$ in the case of the $\mathbb{K}$-process, (1.9) in Theorem 1.5 below. Since these changes do not affect the limiting point process we will ignore this fine point. Some properties of the kernel are given in Sect. 3. Notice that the scaling in the theorems below could have been derived from the scaling used in the limit of the $\mathbb{K}$-kernel to the tacnode process, combined with the way the weight $a \to 1$.

The main statement of the paper reads as follows.

Theorem 1.4 *Let the size of the Aztec diamonds be equal to n. Suppose that when n tends to infinity, the overlap $\rho = n - 2m$ is finite and the a, the weight of each vertical domino, tends* 1 *in the following way:*

$$a = 1 - \frac{\beta}{\sqrt{n/2}}, \quad \textit{with } \beta \in \mathbb{R} \textit{ fixed.}$$

The coordinates (ξ, η) *are scaled as follows,*

$$\xi_i = 2(n - u_i),\ \eta_i = 2t + 2[y_i\sqrt{t}] - 1, \quad \text{with } u_i \in \mathbb{Z},\ y_i \in \mathbb{R}. \tag{1.6}$$

where we set $t = [n/2]$. *With this scaling, the following limit holds:*

$$\lim_{n\to\infty} (-a)^{(\eta_1-\eta_2)/2}(-\sqrt{t})^{(\xi_1-\xi_2)/2}\mathbb{L}_{n,\rho}(\xi_1, \eta_1; \xi_2, \eta_2)\sqrt{t} = \mathbb{K}^{\mathrm{tac}}_{\beta,\rho}(u_1, y_1; u_2, y_2). \tag{1.7}$$

We also have that the rescaled $\mathbb{L}$*-particle process converges weakly to the determinantal point process given by the tacnode GUE-minor kernel.*

In the above theorem, note that ξ_i is always even and η_i always odd. When we go from η_i to y_i we first go from the odd integers to the standard integers to get $[y_i\sqrt{t}]$ and then rescale by $\sqrt{t}$ to go to continuous coordinates y_i in the limit. This explains why the correlation kernel is rescaled by just $\sqrt{t}$.

Remember the remark at the end of Sect. 1.2. The $\mathbb{K}$-process induces a process of particles along the consecutive lines $\{\xi = 2s\}$. This is to say the roles of $2r$ and x in the kernel $\mathbb{K}_{n,\rho}$ get reversed from the point of view of scaling: the variable $2r$ turns into the continuous variable y and the variables x into the discrete variable u. The simulations of lower-Fig. 2 show that the lines $\{\xi = 2s\}$ passing through the overlap $A \cap B$ contain long dense stretches of $\mathbb{K}$-particles. But performing a random thinning, one nevertheless is led in the limit to a point process kernel, which turns out to be the same tacnode GUE-minor kernel, except for some shift.

We do not have a transparent explanation of why we get the same limiting kernel. However, a few extra-words here might help. The dots on the south-dominos (green dominos as in Fig. 5) are $\mathbb{L}$-particles, as well as $\mathbb{K}$-particles, whereas the $\mathbb{L}$-particles belonging to east-dominos (blue) get replaced by $\mathbb{K}$-particles belonging to west-dominos (red), showing duality between east and west dominos. Because of the thinning, south dominos become rare and play no role in the $\mathbb{K}$-process. This provides some explanation why, in appropriate limits, both processes lead to the same statistics; the shift by 1 in the u_2-coordinate remains mysterious. This is the content of the next theorem.

Theorem 1.5 *Let* a, n *and* ρ *be as in the previous theorem and consider the same scaling as above, but expressed in the* (x, z)*-coordinates, using the map* (1.1),

$$2x_i = -\rho + 2u_i + 2[y_i\sqrt{t}], \quad 2r_i = 2t + 2[y_i\sqrt{t}]. \tag{1.8}$$

Let the $\mathbb{K}$*-particles be thinned out at the rate* $p_n = 1 - 2/\sqrt{t}$. *We then have the following limit:*

$$\lim_{n\to\infty} (1 - p_n)a^{r_2-r_1}(\sqrt{t})^{x_1-x_2-r_1+r_2}(-1)^{x_1-x_2}\mathbb{K}_{n,\rho}(2r_1, x_1; 2r_2, x_2)\sqrt{t} = \mathbb{K}^{\mathrm{tac}}_{\beta,\rho}(u_2 + 1, y_2; u_1, y_1). \tag{1.9}$$

Interpreted as a weak limit of a point process this means that if we thin the $\mathbb{K}$*-process by removing each* $\mathbb{K}$*-particle independently with probability* p_n, *then the resulting point*

process converges weakly to a determinantal point process given by the correlation kernel on the right hand side of (1.9).

Notice the kernel $\mathbb{K}^{\mathrm{tac}}_{\beta,\rho}$ is the same as the one in Theorem 1.4, except for the shift in u_2 and the flip $u_1 \leftrightarrow u_2$ and $y_1 \leftrightarrow y_2$.

We now explain our results using the relatively large simultations introduced earlier in the paper. The geometry of the level curves for the double Aztec diamond, when $n \to \infty$, looks as in Fig. 1. The $\mathbb{K}$ and $\mathbb{L}$ particle processes have also been plotted for this simulation and is found in Fig. 2. As $n \to \infty$, the particles take continuous values on each line; they are constrained by the same interlacing as in Proposition 1.3.

2 The kernel for the $\mathbb{L}$-process, via Kasteleyn

2.1 The $\mathbb{L}$-particle process

The kernel $\mathbb{L}_{n,\rho}$ for the $\mathbb{L}$-process is given by Eq. (1.2), i.e.,

$$\begin{aligned}\mathbb{L}_{n,\rho}(\xi_1,\eta_1;\xi_2,\eta_2) &= (1+a^2)\mathbb{L}^{(0)}_n(\xi_1,\eta_1;\xi_2,\eta_2)\\ &\quad -(1+a^2)\langle((I-K_n)^{-1}_{\geq n-\rho+1}A_{\xi_1,\eta_1})(.),B_{\xi_2,\eta_2}(.)\rangle_{\geq n-\rho+1},\end{aligned} \tag{2.1}$$

with

$$\begin{aligned}\mathbb{L}^{(0)}_n(\xi_1,\eta_1;\xi_2,\eta_2) &:= -\mathbb{I}_{(\xi_1<\xi_2)}\int_{\Gamma_{0,a}}\frac{dw}{2\pi\mathrm{i}}\,\frac{(1+aw)^{(\eta_1-\eta_2)/2-1}}{(w-a)^{(\eta_1-\eta_2)/2+1}}w^{\frac{\xi_1-\xi_2}{2}}\\ &\quad+\int_{\Gamma_{0,a}}\frac{dz}{(2\pi\mathrm{i})^2}\int_{\Gamma_{0,a,z}}\frac{dw}{w-z}\,\frac{(1+az)^{(\eta_1-1)/2}(z-a)^{n-(\eta_1+1)/2}w^{n-\xi_2/2}}{(1+aw)^{(\eta_2+1)/2}(w-a)^{n-(\eta_2-1)/2}z^{n-\xi_1/2}}\end{aligned}$$

$$K_n(j,k) = \frac{(-1)^{j+k}}{(2\pi\mathrm{i})^2}\int_{\Gamma_{0,a}}dw\int_{\Gamma_{0,a,w}}\frac{dz}{z-w}\,\frac{z^{n-j}(1+aw)^n(w-a)^{n+1}}{w^{n+1-k}(1+az)^n(z-a)^{n+1}},$$

$$\begin{aligned}A_{\xi_1,\eta_1}(k) &= \frac{(-1)^k}{(2\pi\mathrm{i})^2}\int_{\Gamma_{0,a}}dz\int_{\Gamma_{0,a,z}}\frac{dw}{w-z}\,\frac{(1+az)^{(\eta_1-1)/2}(z-a)^{n-(\eta_1+1)/2}w^{n-k}}{(1+aw)^n(w-a)^{n+1}z^{n-\xi_1/2}}\\ &\quad-\frac{(-1)^k}{2\pi\mathrm{i}}\int_{\Gamma_{0,a}}\frac{w^{\xi_1/2-k}}{(1+aw)^{n-(\eta_1-1)/2}(w-a)^{(\eta_1+3)/2}}\,dw\end{aligned}$$

$$\begin{aligned}B_{\xi_2,\eta_2}(k) &= \frac{(-1)^k}{(2\pi\mathrm{i})^2}\int_{\Gamma_{0,a}}dw\int_{\Gamma_{0,a,w}}\frac{dz}{w-z}\,\frac{(1+aw)^n(w-a)^{n+1}z^{n-\xi_2/2}}{(1+az)^{(\eta_2+1)/2}(z-a)^{n-(\eta_2-1)/2}w^{n+1-k}}\\ &\quad+\frac{(-1)^k}{2\pi\mathrm{i}}\int_{\Gamma_{0,a}}(1+az)^{n-(\eta_2+1)/2}(z-a)^{(\eta_2+1)/2}z^{k-1-\xi_2/2}\,dz\end{aligned} \tag{2.2}$$

As was shown in [2] the $\mathbb{K}$-particles form a determinantal point process and the kernel $\mathbb{K}_{n,\rho}$ for the $\mathbb{K}$-process is given in (z,x) coordinates by

$$(-1)^{x-y}\mathbb{K}_{n,\rho}(2r,x;2s,y)=\mathbb{K}_n^0\big(2r,x;2s,y\big) - \Big\langle (\mathbb{I}-K_n)^{-1}_{\geq n-\rho+1} a_{-y,2s}(.), b_{-x,2r}(.)\Big\rangle_{\geq n-\rho+1}, \tag{2.3}$$

where $K_n(j,k)$ is defined as before in (2.2) and where

$$\begin{aligned}
\mathbb{K}_n^0(2r,x;2s,y) &= \mathbb{K}_{n+1}^{\mathrm{OneAzt}}\big(2(n-r+1),m-x+1;2(n-s+1),m-y+1\big)\\
&= -\mathbb{I}_{s<r}(-1)^{x-y}\psi_{2r,2s}(x,y)+S(2r,x;2s,y) \qquad (2.4)\\
a_{x,2s+\epsilon_1}(k) &:= \frac{(-1)^{k-x}}{(2\pi\mathrm{i})^2}\int_{\Gamma_{0,a}}du\int_{\Gamma_{0,a,u}}\frac{dv}{u-v}\,\frac{v^{x+m}}{u^{k+1}}\,\frac{(1+av)^s(1-\frac{a}{v})^{n-s+1-\epsilon_1}}{(1+au)^n(1-\frac{a}{u})^{n+1}}\\
&= \frac{(-1)^{k-x}}{(2\pi\mathrm{i})^2}\int_{\Gamma_{0,a}}dv\int_{\Gamma_{0,a,v}}\frac{du}{u-v}\,\frac{v^{x+m}}{u^{k+1}}\,\frac{(1+av)^s(1-\frac{a}{v})^{n-s+1-\epsilon_1}}{(1+au)^n(1-\frac{a}{u})^{n+1}}\\
&\quad -\frac{(-1)^{k-x}}{2\pi\mathrm{i}}\int_{\Gamma_{0,a}}dv\,\frac{v^{x+m-k-1}}{(1+av)^{n-s}(1-\frac{a}{v})^{s+\epsilon_1}}\\
b_{y,2r+\epsilon_2}(\ell) &:= \frac{(-1)^{\ell-y}}{(2\pi\mathrm{i})^2}\int_{\Gamma_{0,a}}du\int_{\Gamma_{0,a,u}}\frac{dv}{v-u}\,\frac{v^{\ell}}{u^{y+m+1}}\,\frac{(1+av)^n(1-\frac{a}{v})^{n+1}}{(1+au)^r(1-\frac{a}{u})^{n-r+1-\epsilon_2}}\\
&= \frac{(-1)^{l-y}}{(2\pi\mathrm{i})^2}\int_{\Gamma_{0,a}}dv\int_{\Gamma_{0,a,v}}\frac{du}{v-u}\,\frac{v^{l}}{u^{y+m+1}}\,\frac{(1+av)^n(1-\frac{a}{v})^{n+1}}{(1+au)^r(1-\frac{a}{u})^{n-r+1-\epsilon_2}}\\
&\quad +\frac{(-1)^{l-y}}{2\pi\mathrm{i}}\int_{\Gamma_{0,a}}dv\,\frac{(1+av)^{n-r}(1-\frac{a}{v})^{r+\epsilon_2}}{v^{y+m-l+1}} \qquad (2.5)\\
S(2r+\epsilon_1,x;2s+\epsilon_2,y) &:= \frac{(-1)^{x-y}}{(2\pi\mathrm{i})^2}\int_{\Gamma_{0,a}}du\int_{\Gamma_{0,a,u}}\frac{dv}{v-u}\\
&\quad \frac{v^{x-m-1}}{u^{y-m}}\,\frac{(1+au)^s(1-\frac{a}{u})^{n-s+1-\epsilon_2}}{(1+av)^r(1-\frac{a}{v})^{n-r+1-\epsilon_1}}\\
\psi_{2r+\epsilon_1,2s+\epsilon_2}(x,y) &:= \int_{\Gamma_{0,a}}\frac{dz}{2\pi\mathrm{i}z}z^{x-y}\,\frac{(1+az)^{s-r}}{(1-\frac{a}{z})^{s-r+\epsilon_2-\epsilon_1}}.
\end{aligned}$$

A single Aztec diamond of size n leads to a determinantal process as well (see [15]), for which the kernel is given by the following expression:

$$\mathbb{K}_n^{\mathrm{OneAzt}}(2r,x;2s,y)=\frac{(-1)^{x-y}}{(2\pi\mathrm{i})^2}\int_{\gamma_{r_3}}du\int_{\gamma_{r_2}}\frac{dv}{v-u}\,\frac{v^{-x}}{u^{1-y}}\,\frac{(1+au)^{n-s}(1-\frac{a}{u})^s}{(1+av)^{n-r}(1-\frac{a}{v})^r} - \mathbb{I}_{s>r}\psi_{2r,2s}(x,y).$$

It is not immediate to go from knowing the kernel for the $\mathbb{K}$-particle process to the kernel for the $\mathbb{L}$-particles process. To do so we will use the fact that we can get the

inverse Kasteleyn matrix for the dimer version of Double Aztec diamond. The inverse Kasteleyn matrix will be explained in terms of the kernel $\mathbb{K}_{n,\rho}$. Using the inverse Kasteleyn matrix it is possible to show that the $\mathbb{L}$-particles form a determinantal point process and compute the kernel.

2.2 The Kasteleyn matrix

Suppose that $G = (V, E)$ is a bipartite graph. A dimer is an edge and a dimer covering is a subset of edges such that each vertex is incident to only one edge. The dual of the double Aztec diamond is a subset of the square grid graph with a certain boundary condition while a domino tiling of the double Aztec diamond is a dimer covering of its dual graph. Kasteleyn, in [18], introduced a matrix, later named the *Kasteleyn matrix* which one can use to compute the number of domino tilings of the graph. Since the graph in this paper is bipartite, the Kasteleyn matrix is a type of signed weighted (possibly complex entries) adjacency matrix with rows indexed by the black vertices and columns indexed by the white vertices. The sign of the entries is chosen so that the product of the entries of the Kasteleyn matrix for edges surrounding each face is negative. This is called the *Kasteleyn orientation*. We will describe the Kasteleyn matrix for the double Aztec diamond below but first we state Kasteleyn's theorem for bipartite graphs and Kenyon's formula [19].

Suppose that K denotes the Kasteleyn matrix for a finite bipartite graph G.

Theorem 2.1 ([18]) *The number of weighted dimer coverings of G is equal to* $|\det K|$.

Suppose that $E = \{e_i\}_{i=1}^n$ are a collection of distinct edges with $e_i = (b_i, w_i)$, where b_i and w_i denote black and white vertices.

Theorem 2.2 ([19]) *The dimers form a determinantal point process on the edges of G with correlation kernel given by*

$$L(e_i, e_j) = K(b_i, w_i)K^{-1}(w_i, b_j)$$

where $K(b, w) = K_{bw}$ *and* $K^{-1}(w, b) = (K^{-1})_{wb}$

The above theorem means that by knowing the inverse of the Kasteleyn matrix, which we call the *inverse Kasteleyn matrix*, we can derive the correlation kernel of the dominos. We can now introduce the Kasteleyn matrix of the double Aztec diamond.

Let

$$\mathtt{W} = \{(x_1, x_2) : x_1 \in 2\mathbb{Z} + 1, x_2 \in 2\mathbb{Z}\}$$

denote the set of white vertices and let

$$\mathtt{B} = \{(x_1, x_2) : x_1 \in 2\mathbb{Z}, x_2 \in 2\mathbb{Z} + 1\}$$

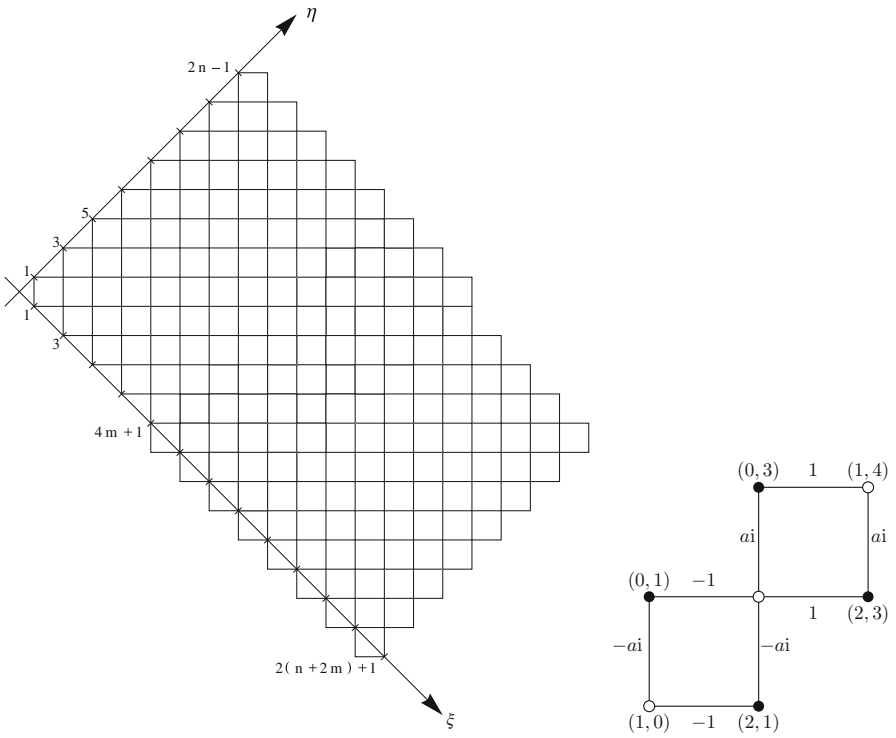

Fig. 10 The *left hand figure* shows the dual graph of the double Aztec diamond with $n = 8$ and $m = 4$ in the (ξ, η) co-ordinates. The *right hand figure* shows the weights, Kasteleyn orientation, *black* and *white* vertices for the two most *left squares*, with (ξ, η)-coordinates

denote the set of black vertices. The dual graph of the double Aztec diamond written in (ξ, η) co-ordinates has white vertices given by

$$\mathtt{W}_{AD} = \left\{(x_1, x_2) \in \mathtt{W} : \begin{array}{l} 1 \le x_1 \le 2(2m+n)+1, 0 \le x_2 \le 2(n-1) \\ \text{or } 1 \le x_1 \le 2n-1, x_2 = 2n \end{array}\right\}$$

and has black vertices given by

$$\mathtt{B}_{AD} = \left\{(x_1, x_2) \in \mathtt{B} : \begin{array}{l} 0 \le x_1 \le 2(2m+n), 1 \le x_2 \le 2n-1 \\ \text{or } 2(2m+1) \le x_1 \le 2(2m+n), x_2 = -1 \end{array}\right\}.$$

We denote by $A_{n,m}$ to be vertex set of the dual graph of the double Aztec diamond with (ξ, η) co-ordinates. Figure 10 shows the dual graph of the double Aztec diamond with $n = 8$ and $m = 4$.

Let K_a denote the Kasteleyn matrix for the double Aztec diamond with entries

$$K_a(\mathtt{b},\mathtt{w}) = \begin{cases} (-1)^{-(b_1+b_2+1)/2}\alpha(r) & \text{if } \mathtt{w} = \mathtt{b} + e_r \\ (-1)^{-(b_1+b_2-1)/2}\alpha(r) & \text{if } \mathtt{w} = \mathtt{b} - e_r \\ 0 & \text{otherwise} \end{cases} \tag{2.6}$$

with $e_1 = (1, 1), e_2 = (-1, 1), \mathtt{b} = (b_1, b_2) \in \mathtt{B}, r = 1, 2, \alpha(1) = 1$ and $\alpha(2) = -a\mathrm{i}$. The choice of sign for the entries of the matrix is the same as [5]. These are chosen so that entries of the inverse Kasteleyn matrix are discrete analytic functions when $a = 1$.

Theorem 2.3 *The entries of inverse Kasteleyn matrix for the double Aztec diamond, K_a, defined by (2.6) are given by*

$$K_a^{-1}(\mathtt{w},\mathtt{b}) = -(-1)^{(w_1-w_2+b_1-b_2+2)/4}\mathbb{K}_{n,\rho} \times \left(b_2+1, \frac{b_2-b_1+2m+1}{2}; w_2+1, \frac{w_2-w_1+2m+1}{2}\right), \tag{2.7}$$

where as before $n - \rho = 2m$.

In other words, using (1.1), $(x, z) \leftrightarrow (\xi, \eta)$,

$$K_a^{-1}(\mathtt{w},\mathtt{b}) = -(-1)^{(w_1-w_2+b_1-b_2+2)/4}\mathbb{K}_{n,\rho}\,(z(\mathtt{b}), x(\mathtt{b}); z(\mathtt{w}), x(\mathtt{b}))$$

so essentially the two kernels are the transpose of each other modulo the co-ordinate transformation (1.1).

The proof of this theorem involves the characterization of K_a^{-1}: $K_a.K_a^{-1} = \mathbb{I}$ and is given in Sect. 6. In order to find such a formula for K_a^{-1} we used a guess following the approach in [5]. More explicitly, using the $\mathbb{K}$ particle correlation kernel one can compute the joint probabilities of $\mathbb{K}$-particles. As these particles correspond t o east and south dominos, this joint probability should be equal to a corresponding formula written in terms of the inverse Kasteleyn matrix by using Theorem 2.2. These two sides can be compared which gives a guess for the inverse Kasteleyn matrix in terms of the $\mathbb{K}$ particle correlation kernel and leads to the formula in the theorem.

Since we now have the inverse Kasteleyn matrix we can use Theorem 2.2 to prove Theorem 1.1. The basic observation is that we have an $\mathbb{L}$-particle at a black vertex b if and only if a dimer covers the edge $(b, b + e_1)$ or the edge $(b, b - e_2)$. By using Theorem 2.3 we can compute the probability of seeing $\mathbb{L}$-particles at given black vertices $b_1, \ldots, b_\ell$ by summing over all the possibilities for the dimers and using Theorem 2.2 and thus deduce the $\mathbb{L}$ kernel, see Sect. 7 for the details.

For general weights and boundary conditions of the square grid, if we define a point process on the black vertices such that a particle is present at a black vertex iff a dimer is incident to that black vertex, from Theorem 2.2, we can recover the particle correlation kernel provided we know the inverse Kasteleyn matrix of the model. In general, the reverse, i.e. to go from the particle correlation kernel to the inverse Kasteleyn matrix, is quite complicated. However, for the double Aztec diamond, we were able to express the

inverse Kasteleyn matrix in terms of the $\mathbb{K}$-kernel. There should also be an analogous formula for the inverse Kasteleyn matrix in terms of the $\mathbb{L}$-kernel. This formula could then be used to give the $\mathbb{K}$-kernel in terms of the $\mathbb{L}$-kernel.

3 The tacnode GUE-minor kernel and its symmetry

Recall from (1.4) the tacnode GUE-Minor kernel, about which we show the following.

Proposition 3.1 *The kernel* $\mathbb{K}^{\mathrm{tac}}_{\beta,\rho}(u_1, y_1; u_2, y_2)$ *is invariant under the involution*

$$u_1 \leftrightarrow \rho - u_2, \qquad y_1 \leftrightarrow -y_2, \tag{3.1}$$

and is a finite rank perturbation of the GUE-minor kernel, as follows[3]*:*

$$\begin{aligned}
&\mathbb{K}^{\mathrm{tac}}_{\beta,\rho}(u_1, y_1; u_2, y_2)\\
&\overset{(*)}{=} \mathbb{K}^{\mathrm{minor}}(u_1, \beta - y_1;\ u_2, \beta - y_2)\\
&\quad +2 \sum_{\lambda=0}^{\max(\rho-1,\rho-1-u_2)} \Big(\big(\mathbb{I} - \mathcal{K}^{\beta}(\lambda-\rho, \kappa-\rho)\big)^{-1} \mathcal{A}^{\beta, y_1-\beta}_{u_1}(\kappa-\rho) \Big)\ \mathcal{B}^{\beta, y_2-\beta}_{u_2}(\lambda-\rho)\\
&\overset{(**)}{=} \mathbb{K}^{\mathrm{minor}}(\rho - u_2, \beta + y_2;\ \rho - u_1, \beta + y_1)\\
&\quad +2 \sum_{\lambda=0}^{\max(\rho-1,u_1-1)} \Big(\big(\mathbb{I} - \mathcal{K}^{\beta}(\lambda-\rho, \kappa-\rho)\big)^{-1} \mathcal{A}^{\beta, -y_2-\beta}_{\rho-u_2}(\kappa-\rho) \Big)\ \mathcal{B}^{\beta, -y_1-\beta}_{\rho-u_1}(\lambda-\rho)
\end{aligned} \tag{3.2}$$

□

Remark 3.2 This symmetry (3.1) is not surprising, since it corresponds to the symmetry of the geometry of the double Aztec diamond.

Proof In order to prove this statement we need the following functions,

$$G(\lambda) = \int_L \frac{d\omega}{2\pi i} e^{2\omega^2 - 4\beta\omega} \omega^{-\lambda-2}, \quad g_y(k) = \int_L \frac{d\omega}{2\pi i} e^{\omega^2 - 2(\beta-y)\omega} \omega^{-k-1}$$
$$H(\kappa) = \int_{\Gamma_0} \frac{d\zeta}{2\pi \mathrm{i}\zeta^{-\kappa}} e^{-2\zeta^2 + 4\beta\zeta}, \qquad h_y(\lambda) = \int_{\Gamma_0} \frac{d\zeta}{2\pi \mathrm{i}\zeta^{-\lambda}} e^{-\zeta^2 + 2(\beta-y)\zeta},$$

and the corresponding operators

$$\mathcal{G}(\kappa, \alpha) f(\alpha) := \sum_{\alpha \geq 0} G(\kappa - \rho + \alpha) f(\alpha)$$
$$\mathcal{H}(\lambda, \alpha) f(\alpha) := \sum_{\alpha \geq 0} H(\lambda - \rho + \alpha) f(\alpha).$$

[3] The inverse $\big(\mathbb{I} - \mathcal{K}^{\beta}(\lambda-\rho, \kappa-\rho)\big)^{-1}$ is taken in the variables $\lambda, \kappa \in \{0, 1, 2, \ldots\}$.

The kernel $\mathcal{K}^\beta$ and its resolvent, and the functions $\mathcal{A}_v^{\beta,y}(\kappa)$ and $\mathcal{B}_u^{\beta,y}(\lambda)$ as in (1.6) can then be expressed as follows,

$$\begin{aligned}
\mathcal{K}^\beta(\lambda,\kappa) &= \sum_{\alpha\geq 0} G(\lambda+\alpha)\, H(\alpha+\kappa), \quad \mathcal{K}_\rho(\lambda,\kappa) := \mathcal{K}^\beta(\lambda-\rho,\kappa-\rho),\\
\mathcal{K}_\rho &= \mathcal{G}\mathcal{H}, \qquad \mathcal{K}_\rho^\top = \mathcal{H}\mathcal{G}, \qquad \text{with } \mathcal{G}^\top = \mathcal{G}\ ,\ \mathcal{H}^\top = \mathcal{H},\\
\mathbb{I}+\mathcal{R}(\lambda,\kappa) &:= (\mathbb{I}-\mathcal{K}_\rho(\lambda,\kappa))^{-1} = \sum_{\alpha\geq 0}\mathcal{K}_\rho^\alpha \qquad (3.3)\\
\mathcal{A}_{u_1}^{\beta,y_1-\beta}(\kappa-\rho) &= g_{-y_1}(\kappa-\rho+u_1) - \sum_{\alpha\geq 0} G(\kappa-\rho+\alpha)h_{y_1}(\alpha-u_1)\\
&= g_{-y_1}(\kappa-\rho+u_1) - \mathcal{G}(\kappa,\cdot)h_{y_1}(\cdot-u_1)\\
\mathcal{B}_{u_2}^{\beta,y_2-\beta}(\lambda-\rho) &= h_{-y_2}(\lambda-\rho+u_2) - \sum_{\alpha\geq 0} H(\lambda-\rho+\alpha)g_{y_2}(\alpha-u_2)\\
&= h_{-y_2}(\lambda-\rho+u_2) - \mathcal{H}(\lambda,\cdot)g_{y_2}(\cdot-u_2)
\end{aligned}$$

Using the definition (1.4) of the kernel and the expressions (3.4), we have the following identities:

$$\begin{aligned}
&\frac{1}{2}\,\mathbb{K}^{\mathrm{tac}}_{\beta,\rho}(u_1,\beta-y_1;u_2,\beta-y_2)\\
&\quad= -\mathbb{I}_{u_1>u_2}2^{u_1-u_2-1}\mathbb{H}^{u_1-u_2}(y_2-y_1) + \sum_{\alpha\geq 0} g_{y_2}(\alpha-u_2)h_{y_1}(\alpha-u_1)\\
&\qquad+\Big\langle(\mathbb{I}+\mathcal{R}(\lambda,\kappa))g_{-y_1}(\kappa-\rho+u_1),\ h_{-y_2}(\lambda-\rho+u_2)\Big\rangle_{\geq 0}\\
&\qquad+\Big\langle\mathcal{H}(\lambda,\alpha)g_{y_2}(\alpha-u_2),\ (\mathbb{I}+\mathcal{R}(\lambda,\kappa))\mathcal{G}(\kappa,\alpha)h_{y_1}(\alpha-u_1)\Big\rangle_{\geq 0}\\
&\qquad-\Big\langle(\mathbb{I}+\mathcal{R}(\lambda,\kappa))g_{-y_1}(\kappa-\rho+u_1),\ \mathcal{H}(\lambda,\alpha)g_{y_2}(\alpha-u_2)\Big\rangle_{\geq 0}\\
&\qquad-\Big\langle(\mathbb{I}+\mathcal{R}(\lambda,\kappa))\mathcal{G}(\kappa,\alpha)h_{y_1}(\alpha-u_1),\ h_{-y_2}(\lambda-\rho+u_2)\Big\rangle_{\geq 0}\\
&\quad= -\mathbb{I}_{u_1>u_2}2^{u_1-u_2-1}\mathbb{H}^{u_1-u_2}(y_2-y_1)\\
&\qquad+\Big\langle g_{-y_1}(\kappa-\rho+u_1),\ (\mathbb{I}+\mathcal{R}^\top(\lambda,\kappa))h_{-y_2}(\lambda-\rho+u_2)\Big\rangle_{\kappa\geq 0}\\
&\qquad+\Big\langle g_{y_2}(\alpha-u_2),\ (\mathbb{I}+\mathcal{H}^T(\mathbb{I}+\mathcal{R})\mathcal{G})h_{y_1}(\alpha'-u_1)\Big\rangle_{\alpha\geq 0}\\
&\qquad-\Big\langle\mathcal{H}^\top(\mathbb{I}+\mathcal{R})g_{-y_1}(\kappa-\rho+u_1),\ g_{y_2}(\alpha-u_2)\Big\rangle_{\alpha\geq 0}\\
&\qquad-\Big\langle(\mathbb{I}+\mathcal{R})\mathcal{G}h_{y_1}(\alpha-u_1),\ h_{-y_2}(\lambda-\rho+u_2)\Big\rangle_{\lambda\geq 0}. \qquad (3.4)
\end{aligned}$$

Given the involution (3.1), all terms in the last expression (3.4) are self-dual, except that the second and third terms interchange, because of the operator identity (see (3.4))

$$\mathbb{I}+\mathcal{H}^\top(\mathbb{I}+\mathcal{R})\mathcal{G} = \mathbb{I}+\mathcal{H}(\mathbb{I}+\mathcal{R})\mathcal{G} = \mathbb{I}+\mathcal{R}^\top$$

and the self-adjointness of $\mathcal{H}^\top(\mathbb{I}+\mathcal{R})$ and $(\mathbb{I}+\mathcal{R})\mathcal{G}$.

To prove the second statement (3.2) on finite perturbation, one notices from (1.6) that the double integral in $\mathcal{B}_u^{\beta,y}(\lambda)$ equals 0 for $\lambda \geq 0$, since the integrand as a function of ζ has no pole at 0 and, similarly the single integral equals 0 for $u+\lambda \geq 0$. Thus $\mathcal{B}_{u_2}^{\beta,y_2-\beta}(\lambda-\rho)=0$ for $\lambda \geq \rho$ and for $\lambda \geq \rho - u_2$. This proves from (1.4), the first equality $\overset{(*)}{=}$. The second equality $\overset{(**)}{=}$ is obtained by the involution (3.1). □

4 Interlacing pattern of the $\mathbb{L}$-process

In this section we prove the interlacing properties as explained in Proposition 1.3. We first need the following Lemma (remember $\rho = n - 2m$).

Lemma 4.1 *The total number of dots along the line $\xi = 2i$ equals the difference of height Δh between the extreme points of that line, as is given by the boundary values of the height function:* [4]

lines $\xi = 2i$	h_{left}	h_{right}	Δh	*# of blue and red dots*
$0 \leq i \leq n-\rho$	n	i	$n-i$	$n-i$ *blue dots*
$n-\rho < i < n$	$\rho+i$	i	ρ	$\rho+i-n$ *red dots to the left of* $n-i$ *blue dots*
$n \leq i \leq 2n-\rho$	$\rho+i$	n	$\rho+i-n$	$\rho+i-n$ *red dots*

Proof The statement on the first row in the table above follows from the fact that the height h along the lines $\xi = 2i$ for $0 \leq i \leq n-\rho$ decreases from $h_{\text{left}} = n$ to $h_{\text{right}} = i$ for $0 \leq i \leq n-\rho$ (going from left to right) and from the fact that each decrease of height by 1 produces a dot. The same statement holds for the range on the third line of the table by the obvious symmetry consisting of flipping the figure about the middle of the ξ-axis and the middle of the η-axis. Also note that the heights of the B-level curves range over the half-integers from $n+1/2$ to $2n-1/2$. Therefore the lines $\xi = 2i$ for $0 \leq i \leq n-\rho$, which have height at most n, will never intersect those lower-level lines and vice-versa, showing that on the first line (resp. last line) of the table above only blue (red resp.) dots appear.

In the overlap region of the two diamonds, the boundary values of the height function show that h_{left}, h_{right} and $\Delta h = h_{\text{left}} - h_{\text{right}}$ is as indicated in the table. Moreover, since the height of the B-level curves is $\geq n+1/2$ and the height of the A-level curves is $\leq n-1/2$, the red dots are all to the left of the blue dots along the lines $\xi = 2(n-\rho)$ up to $2n$, with numbers as indicated in the table. □

Lemma 4.2 *Let the lines $\xi = 2k$ and $\xi = 2k+2$ for $0 \leq k \leq n-1$ have $\ell - 1$ dots starting from the right boundary. Then the ℓth dot on the line $\xi = 2k+2$ must be to the left of or coincide with the ℓth dot on the line $\xi = 2k$.*

[4] A dot-particle x is to the right of a dot-particle y means $\eta(x) \geq \eta(y)$.

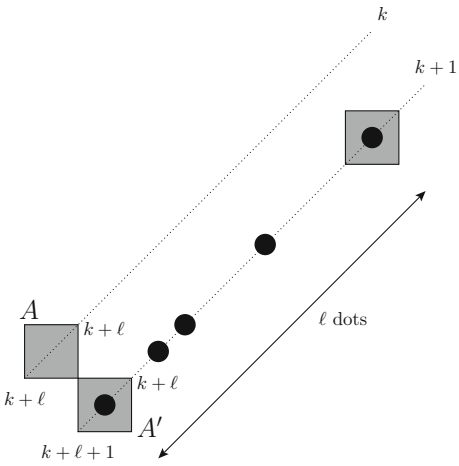

Fig. 11 Assume the ℓth dot on the line $\xi = 2k + 2$ (counted from the *right*) appears in A', and assume no dot in the *square* A, then the height of A must be as indicated

Proof Note that the right most point of the double Aztec diamond on the line $\xi = 2i$ has height i, provided $0 \leq i \leq n$. Therefore, if there are ℓ dots on the line $\xi = 2k+2$, counting from the right hand boundary, then the left-lower vertex of the square A', containing the ℓth dot, has height $k + \ell + 1$; see Fig. 11. Consider two cases:

(i) Assuming no dot in the corresponding square A on the line $\xi = 2k$, then the only way to cover the squares A and A' with domino's such that A' carries a dot and not A, is given by the four upper configurations of Fig. 12; putting in the heights forces the height of the left-lower and right-upper vertices of the square A to be $k + \ell$ as indicated in Fig. 11. This shows there must be ℓ dots on the line $\xi = 2k$ strictly to the right of the square A. So, the ℓth dot on the line $\xi = 2k + 2$ must strictly be to the left of the ℓth dot on the line $\xi = 2k$, at least if A contains no dot.

(ii) Assume a dot in A on the line $\xi = 2k$; the only way for this to occur is given by the four lower configurations of Fig. 12. From them one deduces that, if the height of the lower-left corner of A' is $k + \ell + 1$, then the height of the lower-left corner of A must be $k + \ell$ or $k + \ell + 1$. In the former case (i.e., $k + \ell$), the dots in A and A' are the ℓth ones from the right, proving the claim; in the latter case (i.e., $k + \ell + 1$), the dot in A is the $\ell + 1$st one and the dot in A' the ℓth one. So, the ℓth dot on the line $\xi = 2k$ is to the right of the ℓth one on the line $\xi = 2k + 2$. □

We now give the proof of Proposition 1.3.

Proof of Proposition 1.3 Consider two consecutive lines $\xi = 2\alpha$ and $\xi = 2\alpha + 2$ through blue dots, with the squares A and B, containing each a dot and no dot in between A and B; see Fig. 13. This is to say, the level of the line $\xi = 2\alpha$ goes down from k to $k - 1$ within square A, stays flat in between A and B and then goes down from $k - 1$ to $k - 2$ within square B. We now consider the line $\xi = 2\alpha + 2$ between the two corresponding squares A' and B', with same η coordinates as A and B respectively.

We show there must be at least one dot in between the squares A' and B', possibly including A' or B'. One checks there are exactly six configurations with a dot in the

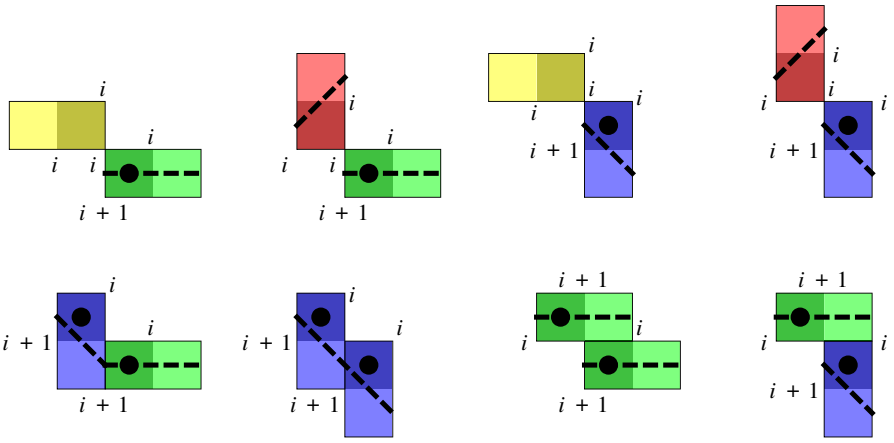

Fig. 12 The *four upper* configurations are the only coverings of A and A' of Fig. 11, with A' carrying a dot and not A. The *four lower* configurations are the only coverings of A and A', with both A and A' carrying a dot

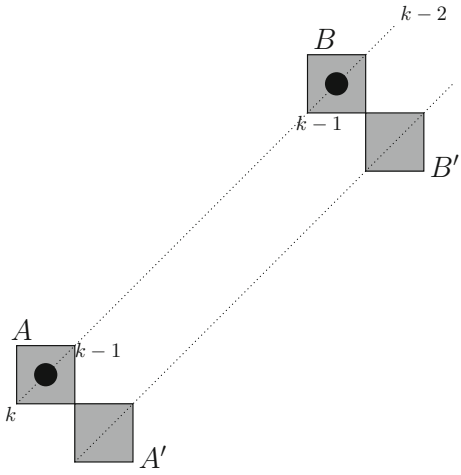

Fig. 13 Between the two *gray squares* labeled A and B the height function stays constant; therefore the line between A and B contains no dots

upper-left square; see Fig. 14. Superimposing any of the four upper configurations on (A, A') or (B, B') will give a dot in A' or B'. Assuming no dot, neither at A', nor at B', the configuration (A, A') or (B, B') at Fig. 13 can be covered by any combination of configurations (I) and (II) in Fig. 14. Indeed,

(A, A')	(B, B')
$\mathrm{I}(i = k-1)$	$\mathrm{I}(i = k-2)$
$\mathrm{I}(i = k-1)$	$\mathrm{II}(j = k-2)$
$\mathrm{II}(j = k-1)$	$\mathrm{I}(i = k-2)$
$\mathrm{II}(j = k-1)$	$\mathrm{II}(j = k-2)$

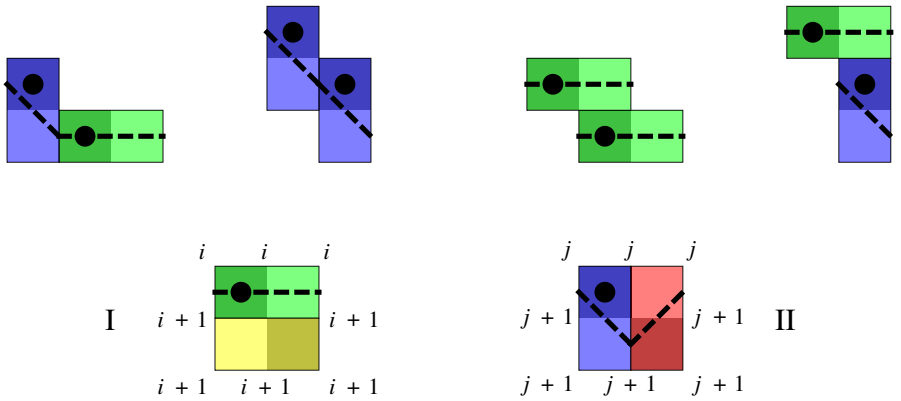

Fig. 14 Let the *squares* A and A' (as in Fig. 13) each contain a dot, then the four *upper figures* are the only possible covers of (A, A'). If A contains a dot and A' does not, then the two *lower figures* are the only possible coverings

In all four cases, the difference in height between the lower-left vertex of A', having height k, and the upper-right vertex of B', having height $k-1$, will always $= 1$, thus creating a jump in between and thus one dot. So in all cases, there will be at least one dot in one of the squares on the segment (A', B'), including possibly on the extremities.

Finally, this fact together with Lemma 4.1 on the number of blue and red dots and Lemma 4.2 imply the interlacing, with regard to the η-coordinate. □

5 Scaling limit of the $\mathbb{L}$ and $\mathbb{K}$-processes

In this section we will prove Theorem 1.4 and Theorem 1.5. Let $\delta \in \{0, 1\}$, where $\delta = 0$ will correspond to the $\mathbb{L}$-kernel and $\delta = 1$ to the $\mathbb{K}$-kernel. We will ignore the integer parts in the scaling (1.6) and (1.8). This makes no essential difference but simplifies the notation. Set

$$f_{t,\delta}(u_1, y_1;\ u_2, y_2) = (-a)^{(y_2-y_1)\sqrt{t}}(-\sqrt{t})^{u_2-u_1}(\sqrt{t})^{1-2\delta}(-1)^{\delta}.$$

Then the prefactor in (1.7) for the $\mathbb{L}$-kernel can be written

$$(-a)^{(\eta_1-\eta_2)/2}(-\sqrt{t})^{(\xi_1-\xi_2)/2}\sqrt{t} = a^{2(y_1-y_2)\sqrt{t}} f_{t,0}(u_1, y_1; u_2, y_2)$$

and the prefactor for the $\mathbb{K}$-kernel in (1.9) is

$$\begin{aligned} &a^{r_2-r_1}(\sqrt{t})^{x_1-x_2+r_2-r_1}(-1)^{x_1-x_2} \\ &= a^{2(y_2-y_1)\sqrt{t}}(-a)^{(y_1-y_2)\sqrt{t}}(-\sqrt{t})^{u_1-(u_2+1)}(-\sqrt{t}) \\ &= a^{2(y_2-y_1)\sqrt{t}} f_{t,1}(u_2+1, y_2;\ u_1, y_1). \end{aligned}$$

Define

$$C^{(1)}_{2t+\epsilon,\rho,\delta}(u_1,y_1;u_2,y_2) = -f_{t,\delta}(u_1,y_1;\,u_2,y_2)(1+a^2)\left((1-\delta)\mathbb{I}_{u_2<u_1}+\delta\mathbb{I}_{y_1<y_2}\right) \times \frac{1}{2\pi \mathrm{i}}\int_{\Gamma_{0,a}} \frac{(1+aw)^{(y_1-y_2)\sqrt{t}-1+\delta}}{(w-a)^{(y_1-y_2)\sqrt{t}+1-\delta}} w^{u_2-u_1}\,dw,$$

$$C^{(2)}_{2t+\epsilon,\rho,\delta}(u_1,y_1;u_2,y_2) = f_{t,\delta}(u_1,y_1;u_2,y_2) \times \frac{(1+a^2)}{(2\pi \mathrm{i})^2}\int_{\Gamma_{0,a}} dz \int_{\Gamma_{0,a,z}} \frac{dw}{w-z}\frac{w^{u_2}(1+az)^{t+y_1\sqrt{t}-1+\delta}(z-a)^{t-y_1\sqrt{t}+\epsilon+\delta}}{z^{u_1}(1+aw)^{t+y_2\sqrt{t}}(w-a)^{t-y_2\sqrt{t}+1+\epsilon}}$$

and

$$C^{(3)}_{2t+\epsilon,\rho,\delta}(u_1,y_1;u_2,y_2) = -f_{t,\delta}(u_1,y_1;u_2,y_2)(1+a^2) \times \left\langle ((I-K_{2t+\epsilon})^{-1}_{\geq 2t+\epsilon-\rho+1} A_{4t+2\epsilon-2u_1,2t+2y_1\sqrt{t}-1,\delta})(.), B_{4t+2\epsilon-2u_2,2t+2y_2\sqrt{t}-1}(.)\right\rangle_{\geq 2t+\epsilon-\rho+1},$$

where

$$\begin{aligned} &A_{4t+2\epsilon-2u_1,2t+2y_1\sqrt{t}-1,\delta}(k) \\ &= -\frac{(-1)^k}{2\pi \mathrm{i}}\int_{\Gamma_{0,a}} \frac{w^{2t+\epsilon-u_1-k}}{(1+aw)^{t+\epsilon-y_1\sqrt{t}+1-\delta}(w-a)^{t+y_1\sqrt{t}+1-\delta}}\,dw \\ &\quad +\frac{(-1)^k}{(2\pi \mathrm{i})^2}\int_{\Gamma_{0,a}} dz \int_{\Gamma_{0,a,z}} \frac{dw}{w-z}\frac{w^{2t+\epsilon-k}(1+az)^{t+y_1\sqrt{t}-1+\delta}(z-a)^{t-y_1\sqrt{t}+\epsilon+\delta}}{z^{u_1}(1+aw)^{2t+\epsilon}(w-a)^{2t+\epsilon+1}}, \end{aligned} \tag{5.1}$$

which is a slight modification of $A_{\xi_1,\eta_1}(k)$ in (2.2), and where $B_{\xi_2,\eta_2}(k)$ and $K_{2t+\epsilon}$ are as given in (2.2). With these definitions it follows from (2.1) that

$$\begin{aligned} &(-a)^{(\eta_1-\eta_2)/2}(-\sqrt{t})^{(\xi_1-\xi_2)/2}\mathbb{L}_{2t+\epsilon,\rho}(\xi_1,\eta_1;\xi_2,\eta_2)\sqrt{t} \\ &= a^{2(y_1-y_2)\sqrt{t}}(C^{(1)}_{2t+\epsilon,\rho,0}+C^{(2)}_{2t+\epsilon,\rho,0}+C^{(3)}_{2t+\epsilon,\rho,0})(u_1,y_1;u_2,y_2), \end{aligned} \tag{5.2}$$

if we have the scaling (1.6). Similarly, it follows from (2.3) that

$$\begin{aligned} &(1-p_n)a^{r_2-r_1}(\sqrt{t})^{x_1-x_2+r_2-r_1}(-1)^{x_1-x_2}\mathbb{K}_{2t+\epsilon,\rho}(2r_1,x_1;2r_2,x_2) \\ &= \frac{2}{1+a^2}a^{2(y_2-y_1)\sqrt{t}}\left(\left(C^{(1)}_{2t+\epsilon,\rho,1}+C^{(2)}_{2t+\epsilon,\rho,1}+C^{(3)}_{2t+\epsilon,\rho,1}\right)(u_2+1,y_2;u_1,y_1)\right). \end{aligned} \tag{5.3}$$

We will now use (5.2) to prove (1.7). The proof of (1.9) from (5.3) is completely analogous since the change from $\delta = 0$ to $\delta = 1$ has no effect in the limit. Note that

$a^{2(y_1-y_2)\sqrt{t}} \to e^{2\beta(y_2-y_1)}$ as $t \to \infty$ since $a = 1 - \beta/\sqrt{t}$. We see that (1.7) follows from

$$\lim_{t\to\infty} \sum_{i=1}^{3} C^{(i)}_{2t+\epsilon,\rho,0}(u_1, y_1;\ u_2, y_2) = e^{2\beta(y_1-y_2)} \mathbb{K}_{\beta,\rho}(u_1, y_1;\ u_2, y_2). \tag{5.4}$$

Let $\mathcal{C}_1$ be the positively oriented unit circle and let $\mathcal{C}_2 = \mathcal{C}_2' + \mathcal{C}_2''$, where $\mathcal{C}_2'$ consists of two infinite line segments $t \to \beta + \mathrm{i}t$, $t \in (-\infty, -2] \cup [2, \infty)$, and $\mathcal{C}_2''$ is a smooth curve that goes from $\beta - 2\mathrm{i}$ to $\beta + 2\mathrm{i}$ to the right of $\mathcal{C}_1$, see Fig. 15.

Let $\overline{\mathcal{C}_2}$ be $\mathcal{C}_2$ reflected through the origin.

Set

$$G_{x,t}(\zeta) = \left(\frac{a^{-1} - \zeta/\sqrt{t}}{a + \zeta/\sqrt{t}}\right)^{x\sqrt{t}}$$

and

$$F_{x,t}(\zeta) = \left(a^{-1} - \zeta/\sqrt{t}\right)^{t+x\sqrt{t}} \left(a + \zeta/\sqrt{t}\right)^{t-x\sqrt{t}}$$

so that $F_{x,t}(\zeta) = F_{0,t}(\zeta) G_{x,t}(\zeta)$. Also, we write

$$g_{x,\beta}(\zeta) = e^{2x(\beta-\zeta)}, \text{ and } f_\beta(\zeta) = e^{2\beta\zeta-\zeta^2}.$$

The next lemma contains the estimates we need.

Fig. 15 The contour paths

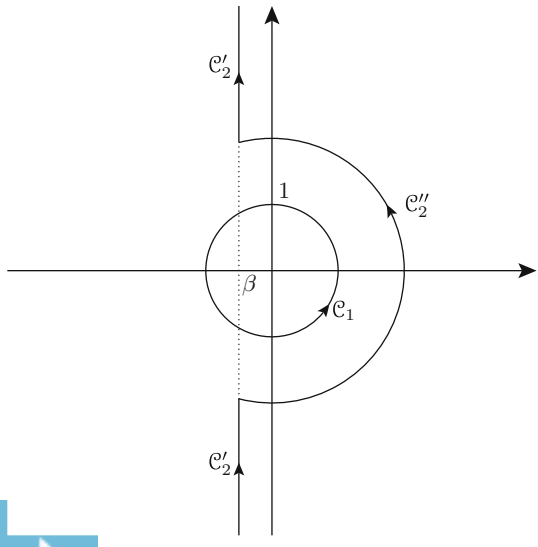

Lemma 5.1 *Fix $A > 0$, $\beta \in \mathbb{R}$ and $k \geq 1$. There is a t_0 and a constant C such that for all $t \geq t_0$, $x \in [-A, A]$, $s \in \mathbb{R}$ and $\zeta \in \mathcal{C}_1 \cup \mathcal{C}_2''$ we have the following estimates*

$$\frac{1}{|F_{x,t}(\beta + \mathrm{i}s)|} \leq \frac{1}{1 + s^{2k}/2^k k!}, \tag{5.5}$$

$$\left| \frac{G_{x,t}(\zeta)}{g_{x,\beta}(\zeta)} - 1 \right| \leq \frac{C}{\sqrt{t}}, \tag{5.6}$$

and

$$\left| \frac{F_{0,t}(\zeta)}{f_\beta(\zeta)} - 1 \right| \leq \frac{C}{\sqrt{t}}. \tag{5.7}$$

Proof We have, since $a = 1 - \beta/\sqrt{t}$, that

$$|F_{x,t}(\beta + \mathrm{i}s)| = \left| a^{-1} - \frac{\beta + \mathrm{i}s}{\sqrt{t}} \right|^{t + x\sqrt{t}} \left| a + \frac{\beta + \mathrm{i}s}{\sqrt{t}} \right|^{t - x\sqrt{t}}.$$

Now,

$$\left| a + \frac{\beta + \mathrm{i}s}{\sqrt{t}} \right|^2 = 1 + \frac{s^2}{t}$$

and

$$\left| a^{-1} - \frac{\beta + \mathrm{i}s}{\sqrt{t}} \right|^2 = \left(\frac{1}{1 - \beta/\sqrt{t}} - \beta\sqrt{t} \right)^2 + \frac{s^2}{t} \geq 1 + \frac{s^2}{t}$$

when t is large enough. Thus,

$$|F_{x,t}(\beta + \mathrm{i}s)| \geq \left(1 + \frac{s^2}{t} \right)^{\frac{1}{2}(t + x\sqrt{t})} \left(1 + \frac{s^2}{t} \right)^{\frac{1}{2}(t - x\sqrt{t})} = \left(1 + \frac{s^2}{t} \right)^t.$$

By the binomial theorem, for $1 \leq k \leq t/2$

$$\left(1 + \frac{s^2}{t} \right)^t = 1 + \sum_{r=1}^{t} \frac{t \ldots (t - r + 1)}{t^r r!} s^{2r} \geq 1 + \frac{t \ldots (t - k + 1)}{t^k k!} s^{2k}$$

$$\geq 1 + \frac{(t/2)^k}{t^k k!} s^{2k} = 1 + \frac{s^{2k}}{2^k k!}.$$

This proves (5.5). Note that $\mathcal{C}_1 \cup \mathcal{C}_2''$ is a fixed compact set. The estimates (5.6) and (5.7) follow from the inequalities

$$\left| x\sqrt{t}\log(a+\zeta/\sqrt{t}) - x(\zeta-\beta) \right| \le \frac{C}{\sqrt{t}},$$
$$\left| x\sqrt{t}\log(a^{-1}-\zeta/\sqrt{t}) - x(\beta-\zeta) \right| \le \frac{C}{\sqrt{t}},$$

and

$$\left| t\log(a^{-1}-\zeta/\sqrt{t})(a+\zeta/\sqrt{t}) - (2\zeta\beta-\zeta^2) \right| \le \frac{C}{\sqrt{t}},$$

for sufficiently large t, which in turn follow from Taylor's theorem. □

Consider first $C^{(1)}_{2t+\epsilon,\rho,0}$. The case $y_1 = y_2$ is special. In this case we obtain

$$\begin{aligned}
&C^{(1)}_{2t+\epsilon,\rho,0}(u_1, y_1; u_2, y_2) \\
&\quad = -(-\sqrt{t})^{u_2-u_1}\sqrt{t}\mathbb{I}_{u_2<u_1}\frac{1+a^2}{2\pi \mathrm{i}}\int_{\Gamma_{0,a}} \frac{w^{u_2-u_1}}{(1+aw)(w-a)}\,dw \\
&\quad = (-\sqrt{t})^{u_2-u_1}\sqrt{t}\mathbb{I}_{u_2<u_1}\frac{a+1/a}{2\pi \mathrm{i}}\int_{\Gamma_{-a^{-1}}} \frac{w^{u_2-u_1}}{(w+1/a)(w-a)}\,dw \\
&\quad = -(-\sqrt{t})^{u_2-u_1}\sqrt{t}\mathbb{I}_{u_2<u_1}(-1/a)^{u_2-u_1}.
\end{aligned}$$

In the second inequality we deformed the contour through infinity to a contour surrounding $-1/a$. If $u_2 = u_1 - 1$ this equals $-a$ which goes to -1 as $t \to \infty$. If $u_2 < u_1 - 1$ the last expression goes to 0 as $t \to \infty$.

If $y_1 > y_2$ then deforming the contour to $\Gamma_{-1/a}$ shows that $C^{(1)}_{2t+\epsilon,\rho,0} = 0$. Assume that $y_1 < y_2$. Then, for large enough t, since $w = a$ is not a pole,

$$\begin{aligned}
&C^{(1)}_{2t+\epsilon,\rho,0}(u_1, y_1; u_2, y_2) \\
&\quad = -\mathbb{I}_{u_2<u_1}\frac{1+a^2}{2\pi \mathrm{i}}\int_{\Gamma_0}\left(\frac{a^{-1}+w}{a-w}\right)^{(y_1-y_2)\sqrt{t}}\frac{(-w\sqrt{t})^{u_2-u_1}}{(1+aw)(a-w)}(-\sqrt{t})\,dw \\
&\quad = -\mathbb{I}_{u_2<u_1}\frac{1+a^2}{2\pi \mathrm{i}}\int_{\mathcal{C}_1} G_{y_1-y_2,t}(\omega)\frac{\omega^{u_2-u_1}}{(1-a\omega/\sqrt{t})(a+\omega/\sqrt{t})}\,d\omega
\end{aligned}$$

by the change of variables $w = -\omega/\sqrt{t}$. It now follows from Lemma 5.1 that

$$\begin{aligned}
&\lim_{t\to\infty} C^{(1)}_{2t+\epsilon,\rho,0}(u_1, y_1; u_2, y_2) \\
&\quad = -\mathbb{I}_{u_2<u_1} \frac{2}{2\pi \mathrm{i}} \int_{\mathcal{C}_1} e^{2(y_2-y_1)(\omega-\beta)} \frac{d\omega}{\omega^{u_1-u_2}} \\
&\quad = -\mathbb{I}_{u_2<u_1} e^{2\beta(y_1-y_2)} 2^{u_1-u_2} \frac{(y_2-y_1)^{u_1-u_2-1}}{(u_1-u_2-1)!}.
\end{aligned}$$

Thus, for all y_1, y_2,

$$\begin{aligned}
&\lim_{t\to\infty} C^{(1)}_{2t+\epsilon,\rho,0}(u_1, y_1; u_2, y_2) \\
&\quad = -\mathbb{I}_{u_1=u_2+1}\mathbb{I}_{y_1=y_2} - \mathbb{I}_{u_2<u_1}\mathbb{I}_{y_1<y_2} e^{2\beta(y_1-y_2)} 2^{u_1-u_2} \cdot \frac{(y_2-y_1)^{u_1-u_2-1}}{(u_1-u_2-1)!} \\
&\quad = -e^{2\beta(y_1-y_2)} 2^{u_1-u_2} H^{u_1-u_2}(y_2-y_1), \qquad (5.8)
\end{aligned}$$

where

$$H^m(z) = \frac{z^{m-1}}{(m-1)!}\left(\mathbb{I}_{z>0} + \frac{1}{2}\mathbb{I}_{z=0}\right)$$

for $m \geq 1$.

Consider now $C^{(2)}_{2t+\epsilon,\rho,0}$. We can write, using the fact the z contour has no pole at $z = a$ for t large, and by completing the $\overline{\mathcal{C}}_2/\sqrt{t}$ contour with an infinite semi-circle on the right,

$$\begin{aligned}
C^{(2)}_{2t+\epsilon,\rho,0}(u_1, y_1; u_2, y_2) &= \frac{1+a^2}{(2\pi \mathrm{i})^2} \int_{\mathcal{C}_1/\sqrt{t}} dz(-\sqrt{t}) \\
&\times \int_{\overline{\mathcal{C}}_2/\sqrt{t}} \frac{dw}{w-z} \frac{(-w\sqrt{t})^{u_2}(a^{-1}+z)^{t+y_1\sqrt{t}}(a-z)^{t-y_1\sqrt{t}+\epsilon}}{(-z\sqrt{t})^{u_1}(a^{-1}+w)^{t+y_2\sqrt{t}}(a-w)^{t-y_2\sqrt{t}+\epsilon}} \frac{1}{(1+az)(a-w)} \\
&= \frac{1+a^2}{(2\pi \mathrm{i})^2} \int_{\mathcal{C}_1} d\zeta \int_{\mathcal{C}_2} \frac{d\omega}{\omega-\zeta} \frac{\omega^{u_2} F_{y_1,t}(\zeta)}{\zeta^{u_1} F_{y_2,t}(\omega)} \frac{(a+\zeta/\sqrt{t})^{\epsilon}}{(1-a\zeta/\sqrt{t})(a+\omega/\sqrt{t})^{1+\epsilon}}.
\end{aligned}$$

It now follows from Lemma 5.1 that

$$\begin{aligned}
&\lim_{t\to\infty} C^{(2)}_{2t+\epsilon,\rho,0}(u_1, y_1; u_2, y_2) \\
&\quad = \frac{2}{(2\pi \mathrm{i})^2} \int_{\mathcal{C}_1} d\zeta \int_{\mathcal{C}_2} \frac{d\omega}{\omega-\zeta} \frac{\omega^{u_2} f_\beta(\zeta) g_{y_1,\beta}(\zeta)}{\zeta^{u_1} f_\beta(\omega) g_{y_2,\beta}(\omega)} \\
&\quad = e^{2\beta(y_1-y_2)} \frac{2}{(2\pi \mathrm{i})^2} \int_{\mathcal{C}_1} d\zeta \int_{\mathcal{C}_2} \frac{d\omega}{\omega-\zeta} \frac{\omega^{u_2} e^{-\zeta^2+2(\beta-y_1)\zeta}}{\zeta^{u_1} e^{-\omega^2+2(\beta-y_2)\omega}}. \qquad (5.9)
\end{aligned}$$

We choose k in (5.5) so that $2k > u_2$, which gives a uniform t-independent upper bound on $\mathcal{C}'_2$. Combining (5.8) and (5.9) we see that

$$\lim_{t\to\infty}(C^{(1)}_{2t+\epsilon,\rho,0}+C^{(2)}_{2t+\epsilon,\rho,0})(u_1,y_1;u_2,y_2)=e^{2\beta(y_1-y_2)}\mathbb{K}^{\text{minor}}(u_1,\beta-y_1;u_2,\beta-y_2). \tag{5.10}$$

Next, consider

$$\begin{aligned}C^{(3)}_{2t+\epsilon,\rho,0}(u_1,y_1;\,u_2,y_2) &= -(-a)^{(y_2-y_1)\sqrt{t}}(-\sqrt{t})^{u_2-u_1}\sqrt{t}(1+a^2)\\ &\quad\times\sum_{\kappa,\lambda=0}^{\infty}B_{4t+2\epsilon-2u_2,2t+2y_2\sqrt{t}-1}(\lambda+2t+\epsilon-\rho+1)\\ &\quad\times(I-K_{2t+\epsilon})^{-1}_{\geq 2t+\epsilon-\rho+1}(\lambda+2t+\epsilon-\rho+1,\kappa+2t+\epsilon-\rho+1)\\ &\quad\times A_{4t+2\epsilon-2u_1,2t+2y_1\sqrt{t}-1,0}(\kappa+2t+\epsilon-\rho+1),\end{aligned}$$

where $A_{\xi_1,\eta_1,0}$ is given by (5.1),

$$\begin{aligned}&B_{4t+2\epsilon-2u_2,2t+2y_2\sqrt{t}-1}(j)\\ &\quad=\frac{(-1)^j}{2\pi\mathrm{i}}\int_{\Gamma_{0,a}}(1+az)^{t-y_2\sqrt{t}+\epsilon}(z-a)^{t+y_2\sqrt{t}}z^{u_2-1-2t-\epsilon+j}\,dz\\ &\qquad+\frac{(-1)^j}{(2\pi\mathrm{i})^2}\int_{\Gamma_{0,a}}dw\int_{\Gamma_{0,a,w}}\frac{dz}{w-z}\,\frac{z^{u_2}(1+aw)^{2t+\epsilon}(w-a)^{2t+\epsilon}}{w^{2t+\epsilon-j+1}(1+az)^{t+y_2\sqrt{t}}(z-a)^{t-y_2\sqrt{t}+1+\epsilon}}\end{aligned}$$

and

$$K_{2t+\epsilon}(j,k)=\frac{(-1)^{j+k}}{(2\pi\mathrm{i})^2}\int_{\Gamma_{0,a}}dw\int_{\Gamma_{0,a,w}}\frac{dz}{z-w}\,\frac{z^{2t+\epsilon-j}(1+aw)^{2t+\epsilon}(w-a)^{2t+\epsilon+1}}{w^{2t+\epsilon-k+1}(1+az)^{2t+\epsilon}(z-a)^{2t+\epsilon+1}}.$$

Set

$$\begin{aligned}\tilde{A}_{u_1,y_1,0}(\kappa) &= (-a)^{t-y_1\sqrt{t}}(-\sqrt{t})^{-u_1}(\sqrt{t})^{\rho-\kappa-1}\sqrt{t}(-1)^{-\epsilon}\\ &\quad\times A_{4t+2\epsilon-2u_1,2t+2y_1\sqrt{t}-1,0}(\kappa+2t+\epsilon-\rho+1),\\ \tilde{B}_{u_2,y_2}(\lambda) &= (-a)^{y_2\sqrt{t}-t}(-\sqrt{t})^{u_2}(\sqrt{t})^{\lambda-\rho+1}(-1)^{-\epsilon}\\ &\quad\times B_{4t+2\epsilon-2u_2,2t+2y_2\sqrt{t}-1}(\lambda+2t+\epsilon-\rho+1)\end{aligned}$$

and

$$\tilde{K}_{2t+\epsilon}(\lambda,\kappa)=(\sqrt{t})^{\kappa-\lambda}K_{2t+\epsilon}(\lambda+2t+\epsilon-\rho+1,\kappa+2t+\epsilon-\rho+1).$$

Note that the matrix with elements

$$(\sqrt{t})^{\kappa-\lambda}(I-K_{2t+\epsilon})^{-1}_{\geq 2t+\epsilon-\rho+1}(\lambda+2t+\epsilon-\rho+1,\kappa+2t+\epsilon-\rho+1)$$

is the inverse of the matrix with elements $\delta_{\kappa,\lambda}-\tilde{K}_{2t+\epsilon}(\lambda,\kappa)$. Thus,

$$C^{(3)}_{2t+\epsilon,\rho,0}(u_1,y_1;\,u_2,y_2)=-(1+a^2)\sum_{\kappa,\lambda=0}^{\infty}\tilde{B}_{u_2,y_2}(\lambda)(I-\tilde{K}_{2t+\epsilon})^{-1}_{\geq 0}(\lambda,\kappa)\tilde{A}_{u_1,y_1,0}(\kappa) \tag{5.11}$$

and we want to take the limit of this sum. (Note that the sum is finite even in the limit.)

Rewriting in the same way as above we see from (5.1) that

$$\begin{aligned}\tilde{A}_{u_1,y_1,0}(\kappa)&=-\frac{1}{2\pi\mathrm{i}}\int_{\mathcal{C}_2}\frac{\omega^{-\kappa-u_1+\rho-1}}{F_{-y_1,t}(\omega)}\frac{d\omega}{(1-a\omega/\sqrt{t})^{1+\epsilon}(a+\omega/\sqrt{t})}\\&\quad+\frac{1}{(2\pi\mathrm{i})^2}\int_{\mathcal{C}_1}d\zeta\int_{\mathcal{C}_2}\frac{d\omega}{\omega-\zeta}\frac{\zeta^{-u_1}F_{y_1,t}(\zeta)}{\omega^{\kappa+1-\rho}F_{0,t}(\omega)^2}\\&\quad\times\frac{(a+\zeta/\sqrt{t})^{\epsilon}}{(1-a\zeta/\sqrt{t})(a+\omega/\sqrt{t})^{1+\epsilon}(1-a\omega/\sqrt{t})^{\epsilon}}.\end{aligned}$$

Using Lemma 5.1 we can take the limit $t\to\infty$ to get

$$\begin{aligned}\lim_{t\to\infty}\tilde{A}_{u_1,y_1,0}(\kappa)&=-\frac{1}{2\pi\mathrm{i}}\int_{\mathcal{C}_2}\frac{\omega^{-\kappa-u_1+\rho-1}}{f_\beta(\omega)g_{-y_1,\beta}(\omega)}\,d\omega\\&\quad+\frac{1}{(2\pi\mathrm{i})^2}\int_{\mathcal{C}_1}d\zeta\int_{\mathcal{C}_2}\frac{d\omega}{\omega-\zeta}\frac{\zeta^{-u_1}f_\beta(\zeta)g_{y_1,\beta}(\zeta)}{\omega^{\kappa+1-\rho}f_\beta(\omega)^2}\\&=-e^{2\beta y_1}\mathcal{A}^{\beta,y_1-\beta}_{u_1}(\kappa-\rho).\end{aligned} \tag{5.12}$$

Similarly we get

$$\begin{aligned}\tilde{B}_{u_2,y_2}(\lambda)&=\frac{1}{2\pi\mathrm{i}}\int_{\mathcal{C}_1}F_{-y_2,t}(\zeta)\zeta^{u_2+\lambda-\rho}(1-a\zeta/\sqrt{t})^{\epsilon}\,d\zeta\\&\quad+\frac{1}{(2\pi\mathrm{i})^2}\int_{\mathcal{C}_1}d\omega\int_{\mathcal{C}_2}\frac{d\zeta}{\omega-\zeta}\frac{\omega^{\lambda-\rho}F_{0,t}(\omega)^2}{\zeta^{-u_2}F_{y_2,t}(\zeta)}\frac{(a+\omega/\sqrt{t})^{1+\epsilon}(1-a\omega/\sqrt{t})^{\epsilon}}{(a+\zeta/\sqrt{t})^{1+\epsilon}}\end{aligned}$$

and again by Lemma 5.1 we find

$$\lim_{t\to\infty} \tilde{B}_{u_2,y_2}(\lambda) = \frac{1}{2\pi \mathrm{i}} \int_{\mathcal{C}_1} f_\beta(\zeta) g_{-y_2,\beta}(\zeta) \zeta^{u_2+\lambda-\rho}\, d\zeta + \frac{1}{(2\pi \mathrm{i})^2} \int_{\mathcal{C}_1} d\omega \int_{\mathcal{C}_2} \frac{d\zeta}{\omega-\zeta} \frac{\omega^{\lambda-\rho} f_\beta(\omega)^2}{\zeta^{-u_2} f_\beta(\zeta) g_{y_2,\beta}(\zeta)} = e^{-2\beta y_2} \mathcal{B}_{u_2}^{\beta, y_2-\beta}(\lambda-\rho). \tag{5.13}$$

Finally,

$$\tilde{K}_{2t+\epsilon}(\lambda,\kappa) = \frac{1}{(2\pi \mathrm{i})^2} \int_{\mathcal{C}_1} d\omega \int_{\mathcal{C}_2} \frac{d\zeta}{\zeta-\omega} \frac{\omega^{\kappa-\rho} F_{0,t(\omega)^2}}{\zeta^{\lambda-\rho+1} F_{0,t}(\zeta)^2} \frac{(1-a\omega/\sqrt{t})^\epsilon (a+\omega/\sqrt{t})^{\epsilon+1}}{(1-a\zeta/\sqrt{t})^\epsilon (a+\zeta/\sqrt{t})^{\epsilon+1}}$$

and we see from Lemma 5.1 that

$$\lim_{t\to\infty} \tilde{K}_{2t+\epsilon}(\lambda,\kappa) = \frac{1}{(2\pi \mathrm{i})^2} \int_{\mathcal{C}_1} d\omega \int_{\mathcal{C}_2} \frac{d\zeta}{\zeta-\omega} \frac{\omega^{\kappa-\rho} f_\beta(\omega)^2}{\zeta^{\lambda-\rho+1} f_\beta(\zeta)^2} = \mathcal{K}^\beta(\lambda-\rho,\kappa-\rho). \tag{5.14}$$

It now follows from (5.11), (5.12), (5.13) and (5.14) that

$$\lim_{t\to\infty} C^{(3)}_{2t+\epsilon,\rho,0}(u_1,y_1;\ u_2,y_2) = 2e^{2\beta(y_1-y_2)} \langle (I-\mathcal{K}^\beta)^{-1}_{\geq -\rho} \mathcal{A}_{u_1}^{\beta,y_1-\beta}(.),\ \mathcal{B}_{u_2}^{\beta,y_2-\beta}(.)\rangle_{\geq -\rho}.$$

Together with (5.10) this proves (5.4).

It is not difficult to get t-independent bounds on the $\mathbb{L}$-kernel using the same arguments as above and in this way we can show, in a standard manner, that the appropriate Fredholm determinant converges and obtain weak convergence of the $\mathbb{L}$-particle point process. We will not enter into the details.

6 Proof of the inverse Kasteleyn formula

In this section we prove Theorem 2.3. We will use the fact that

$$\mathbb{K}_{n,\rho}\left(b_2+1, \frac{b_2-b_1+2m+1}{2}; w_2+1, \frac{w_2-w_1+2m+1}{2}\right) = -K^{\text{inlier}}_{n,m}\left(b_2+1, \frac{b_2-b_1+2m+1}{2}; w_2+1, \frac{w_2-w_1+2m+1}{2}\right),$$

where the kernel $K^{\text{inlier}}_{n,m}$ is the inlier kernel from [2], dual to $\mathbb{K}_{n,p}$. We will use the form of the inlier kernel that comes directly from the Eynard-Mehta theorem. Let

$$\tilde{\psi}_{2r+\varepsilon_1,2s+\varepsilon_2}(x,y)=\psi_{2r+\varepsilon_1,2s+\varepsilon_2}(x,y)\mathbb{I}_{2r+\varepsilon_1<2s+\varepsilon_2} \tag{6.1}$$

where ψ is defined in (2.5).

Let $\mathtt{w}=(w_1,w_2)\in\mathtt{W},\mathtt{b}=(b_1,b_2)\in\mathtt{B},u_1=w_2+1,u_2=(w_2-w_1+2m+1)/2$, $v_1=b_2+1$, $v_2=(b_2-b_1+2m+1)/2$ and denote

$$\mathrm{sgn}(\mathtt{w},\mathtt{b})=(-1)^{(w_1-w_2+b_1-b_2+2)/4}$$

Define

$$\tilde{f}_1(\mathtt{w},\mathtt{b})=-\mathrm{sgn}(\mathtt{w},\mathtt{b})\tilde{\psi}_{v_1,u_1}(v_2,u_2)$$

and

$$\tilde{f}_2(\mathtt{w},\mathtt{b})=\mathrm{sgn}(\mathtt{w},\mathtt{b})\sum_{i,j=1}^{2m+1}\tilde{\psi}_{v_1,2n+1}(v_2,i-m-1)(A^{-1})_{i,j}\tilde{\psi}_{0,u_1}(j-m-1,u_2)$$

where

$$A=\left(\tilde{\psi}_{0,2n+1}(i-m-1,j-m-1)\right)_{i,j=1}^{2m+1}. \tag{6.2}$$

We then get

$$-(-1)^{(w_1-w_2+b_1-b_2+2)/4}\mathbb{K}_{n,\rho}(v_1,v_2;u_1,u_2)=\tilde{f}_1(\mathtt{w},\mathtt{b})+\tilde{f}_2(\mathtt{w},\mathtt{b})$$

and we want to prove that

$$K_a^{-1}(\mathtt{w},\mathtt{b})=\tilde{f}_1(\mathtt{w},\mathtt{b})+\tilde{f}_2(\mathtt{w},\mathtt{b}).$$

To make the computations simpler, we define T_a and C with

$$K_a(\mathtt{b},\mathtt{w})=-(-1)^{(b_1+b_2-1)/2}T_a(\mathtt{b},\mathtt{w})$$

and

$$\tilde{f}_1(\mathtt{w},\mathtt{b})+\tilde{f}_2(\mathtt{w},\mathtt{b})=-(-1)^{-(b_1+b_2-1)/2}C(\mathtt{w},\mathtt{b}).$$

and we will write

$$f_i(\mathtt{w},\mathtt{b})=-(-1)^{(b_1+b_2-1)/2}\tilde{f}_i(\mathtt{w},\mathtt{b}).$$

Therefore, showing $K_a.(\tilde{f}_1+\tilde{f}_2)=\mathbb{I}$ is equivalent to showing $T_a.C=\mathbb{I}$.

We will use the notation that $\mathtt{b} = (b_1, b_2)$ and $\mathtt{y} = (y_1, y_2)$ are black vertices. We have that

$$(T_a f_i)(\mathtt{b}, \mathtt{y}) = \sum_{\mathtt{w} \sim \mathtt{b}} T_a(\mathtt{b}, \mathtt{w}) f_i(\mathtt{w}, \mathtt{y}) \tag{6.3}$$

for $i \in \{1, 2\}$ where $\mathtt{w} \sim \mathtt{y}$ means that $\mathtt{w}$ is nearest neighbors to $\mathtt{b}$ because $T_a(\mathtt{b}, \mathtt{w}) = 0$ if $\mathtt{b}$ and $\mathtt{w}$ are not nearest neighbors. We can then write

$$(T_a C)(\mathtt{b}, \mathtt{w}) = \sum_{i \in \{1,2\}} (T_a f_i)(\mathtt{b}, \mathtt{y}).$$

The number of terms on the right hand side of Eq. (6.3) is dependent on the location of $\mathtt{b}$ and so we split the computation for finding $T_a C(\mathtt{b}, \mathtt{y})$ into the different locations of $\mathtt{b}$. These are given by

(i) The interior, labeled $\mathcal{I}$,
(ii) The left hand boundary, labeled $\mathcal{L}$,
(iii) The bottom boundary, labeled $\mathcal{B}$,
(iv) The top boundary but not equal to $(2n, 2n-1)$, labeled $\mathcal{T}$ and
(v) The special point, $(2n, 2n-1)$.

The left hand boundary, $\mathcal{L}$, consists of vertices $\mathtt{b} = (0, b_2)$ where $b_2 \in 2\mathbb{Z}+1$ and $1 \le b_2 \le 2n-1$. For $\mathtt{b} \in \mathcal{L}$, we have that $\mathtt{b}$ has two neighboring white vertices given by $\mathtt{b} + e_1$ and $\mathtt{b} - e_2$.

The bottom boundary, $\mathcal{B}$, consists of vertices $\mathtt{b} = (b_1, -1)$ where $b_1 \in 2\mathbb{Z}$ and $4m + 2 \le b_1 \le 4m + 2n$. For $\mathtt{b} \in \mathcal{B}$, we have that $\mathtt{b}$ has two neighboring white vertices given by $\mathtt{b} + e_1$ and $\mathtt{b} + e_2$.

The top boundary, $\mathcal{T}$, consists of vertices $\mathtt{b} = (b_1, 2n-1)$ where $b_1 \in 2\mathbb{Z}$ and $2n + 2 \le b_1 \le 4m + 2n$. For $\mathtt{b} \in \mathcal{T}$, we have that $\mathtt{b}$ has two neighboring white vertices given by $\mathtt{b} - e_1$ and $\mathtt{b} - e_2$.

For the special point, $\mathtt{b} = (2n, 2n-1)$, we have that $\mathtt{b}$ has three neighboring white vertices given by $\mathtt{b} + e_2$, $\mathtt{b} - e_2$ and $\mathtt{b} - e_1$.

The interior, $\mathcal{I}$, is given by the remaining vertices. For $\mathtt{b} \in \mathcal{I}$, we have that $\mathtt{b}$ has four neighboring white vertices given by $\mathtt{b} \pm e_r$ for $r \in \{1, 2\}$.

In each of the above cases, we evaluate (6.3). Due to the formulas for f_1 and f_2 being rather complicated, we used computer algebra to help with the computations. We give the calculation for the first case with full details and for the remaining cases, we provide an overview of the main steps. We now proceed with checking the above cases.

6.1 The interior

Using (2.6) and the definition of $T_a(\mathtt{b}, \mathtt{w})$, we have that for $b \in \mathcal{I}$

$$T_a(\mathtt{b}, \mathtt{w}) = \begin{cases} \pm 1 & \text{if } \mathtt{w} = \mathtt{b} \pm e_1 \\ \mp ai & \text{if } \mathtt{w} = \mathtt{b} \pm e_2 \\ 0 & \text{otherwise.} \end{cases}$$

When $\mathtt{b} \in \mathcal{I}$ and $\mathtt{y} \in \mathtt{B}_{AD}$, we have that (6.3) reads

$$T_a f_i(\mathtt{b}, \mathtt{y}) = f_i(\mathtt{b} + e_1, \mathtt{y}) - f_i(\mathtt{b} - e_1, \mathtt{y}) + (f_i(\mathtt{b} - e_2, \mathtt{y}) - f_i(\mathtt{b} + e_2, \mathtt{y}))a\mathrm{i} \tag{6.4}$$

for $i \in \{1, 2\}$.

We first simplify (6.4) for $i = 1$. We can expand out the definition of f_1 in terms of $\tilde{\psi}$. This means that we can rewrite (6.4) for $i = 1$ in terms of $\tilde{\psi}$. We obtain

$$\begin{aligned} T_a f_1(\mathtt{b}, \mathtt{y}) = &-(-1)^{(b_1 - b_2 + y_1 - y_2)/4} \mathrm{i}^{y_1 + y_2} \\ &\times \left(a\tilde{\psi}_{y_2+1, b_2}\left(\frac{2m + 1 - y_1 + y_2}{2}, \frac{2m - 1 - b_1 + b_2}{2}\right)\right. \\ &+ \tilde{\psi}_{y_2+1, b_2}\left(\frac{2m + 1 - y_1 + y_2}{2}, \frac{2m + 1 - b_1 + b_2}{2}\right) \\ &- \tilde{\psi}_{y_2+1, b_2+2}\left(\frac{2m + 1 - y_1 + y_2}{2}, \frac{2m + 1 - b_1 + b_2}{2}\right) \\ &\left. + a\tilde{\psi}_{y_2+1, b_2+2}\left(\frac{2m + 1 - y_1 + y_2}{2}, \frac{2m + 3 - b_1 + b_2}{2}\right)\right) \end{aligned} \tag{6.5}$$

where $\tilde{\psi}$ is defined in (6.1). We shall evaluate $T_a f_1(\mathtt{b}, \mathtt{w})$ in three cases: $b_2 = y_2$, $b_2 > y_2$ and $b_2 < y_2$.

For $y_2 = b_2$, we only need to consider the last two terms of (6.5) because the first two terms involving $\tilde{\psi}$ are zero by (6.1). Using (6.1), we can rewrite (6.5) in terms of ψ and hence write each expression as an integral. We find for $b_2 = y_2$

$$\begin{aligned} T_a f_1(\mathtt{b}, \mathtt{y}) &= (-1)^{\frac{b_1 + y_1}{4}} \mathrm{i}^{y_1} \left(\psi_{y_2+1, y_2+2}\left(\frac{2m + 1 - y_1 + y_2}{2}, \frac{2m + 1 - b_1 + y_2}{2}\right)\right. \\ &\quad \left. - a\psi_{y_2+1, y_2+2}\left(\frac{2m + 1 - y_1 + y_2}{2}, \frac{2m + 3 - b_1 + y_2}{2}\right)\right) \\ &= \frac{(-1)^{\frac{b_1 + y_1}{4}} \mathrm{i}^{y_1}}{2\pi \mathrm{i}} \int_{\Gamma_{0,a}} \left(-\frac{w^{\frac{1}{2}(b_1 - y_1)}}{a - w} + \frac{a w^{\frac{1}{2}(b_1 - y_1 - 2)}}{a - w} \right) dw \\ &= \frac{(-1)^{\frac{b_1 + y_1}{4}} \mathrm{i}^{y_1}}{2\pi \mathrm{i}} \int_{\Gamma_{0,a}} w^{\frac{b_1 - y_1 - 2}{2}} dw \\ &= \begin{cases} \mathrm{i}^{2y_1} = 1 & \text{if } b_1 = y_1 \\ 0 & \text{otherwise} \end{cases} \end{aligned}$$

because $y_1 \in 2\mathbb{Z}$.

As both $\mathtt{b}$ and $\mathtt{y}$ are black vertices we have that b_2 and y_2 are both odd integers. Therefore, the condition that $b_2 > y_2$ is equivalent to $b_2 > y_2 + 1$. For $b_2 > y_2$, all four terms of (6.5) involving $\tilde{\psi}$ are nonzero and each term can be rewritten using ψ.

We find that for $b_2 > y_2$

$$\begin{aligned} T_a f_1(\mathtt{b},\mathtt{y}) = &-(-1)^{(b_1-b_2+y_1-y_2)/4}\mathrm{i}^{y_1+y_2} \\ &\times \left(a\psi_{y_2+1,b_2}\left(\frac{2m+1-y_1+y_2}{2}, \frac{2m-1-b_1+b_2}{2}\right)\right. \\ &+\psi_{y_2+1,b_2}\left(\frac{2m+1-y_1+y_2}{2}, \frac{2m+1-b_1+b_2}{2}\right) \\ &-\psi_{y_2+1,b_2+2}\left(\frac{2m+1-y_1+y_2}{2}, \frac{2m+1-b_1+b_2}{2}\right) \\ &\left.+ a\psi_{y_2+1,b_2+2}\left(\frac{2m+1-y_1+y_2}{2}, \frac{2m+3-b_1+b_2}{2}\right)\right) \end{aligned} \tag{6.6}$$

To evaluate (6.6), we need to evaluate an expression of the form

$$\begin{aligned} &a\psi_{2r,2s+1}(x_1,x_2) + \psi_{2r,2s+1}(x_1,x_2+1) \\ &\quad -\psi_{2r,2s+3}(x_1,x_2+1) + a\psi_{2r,2s+3}(x_1,x_2+2) \end{aligned} \tag{6.7}$$

for $r, s, x_1, x_2 \in \mathbb{Z}$. We can expand (6.7) in terms of its integral decomposition and combine all the terms under one integral. We obtain

$$\oint_{\Gamma_{0,a}} \frac{dz}{2\pi\mathrm{i}} z^{x_1-x_2} \frac{(1+az)^{s-r}}{(1-\frac{a}{z})^{s-r+1}} \left(a + \frac{1}{z} - \frac{z^{-1}(1+az)}{1-\frac{a}{z}} + \frac{az^{-2}(1+az)}{1-\frac{a}{z}} \right).$$

In the above equation, the term inside the parenthesis is zero. This means we can write

$$\begin{aligned} &a\tilde{\psi}_{2r,2s+1}(x_1,x_2) + \tilde{\psi}_{2r,2s+1}(x_1,x_2+1) \\ &\quad -\tilde{\psi}_{2r,2s+3}(x_1,x_2+1) + a\tilde{\psi}_{2r,2s+3}(x_1,x_2+2) = 0 \quad \text{for } r < s. \end{aligned} \tag{6.8}$$

Using the relation in (6.8), we have that right hand side of (6.6) is equal to zero for $b_2 > y_2$ which means that $T_a f_1(\mathtt{b},\mathtt{w}) = 0$ for $b_2 > y_2$.

As b_2 and y_2 are both odd integers, the condition that $b_2 < y_2$ is equivalent to $b_2 + 1 < y_2$. We can expand (6.5) using the definition of $\tilde{\psi}$ given in (6.1) and we find that all the terms of (6.5) are equal to zero. Therefore, we have that $T_a f_1(\mathtt{b},\mathtt{w}) = 0$ for $b_2 < y_2$.

We have shown that for $b \in \mathcal{I}$

$$T_a f_1(\mathtt{b},\mathtt{y}) = \begin{cases} 1 & \text{if } \mathtt{b} = \mathtt{y}, \\ 0 & \text{otherwise.} \end{cases}$$

For the term $T_a f_2(\mathtt{b},\mathtt{y})$, using (6.4) we can write $T_a f_2(\mathtt{b},\mathtt{y})$ under one sum. We obtain

$$\begin{aligned} T_a f_2(\mathtt{b},\mathtt{y}) = (-1)^{\frac{b_1-b_2+y_1-y_2}{4}} \mathrm{i}^{y_1+y_2} \sum_{i,j=1}^{2m+1} (A^{-1})_{ij} \\ \times \tilde{\psi}_{1+y_2,2n+1}\left(\frac{2m+1-y_1+y_2}{2}, i-m-1\right) \\ \times \Delta_{\mathcal{I}}\tilde{\psi}_{0,b_2+1}\left(j-m-1, \frac{2m+2-b_1+b_2}{2}\right) \end{aligned}$$

where

$$\begin{aligned} \Delta_{\mathcal{I}}\tilde{\psi}_{0,b_2+1}\left(j-m-1, \frac{2m+2-b_1+b_2}{2}\right) = a\tilde{\psi}_{0,b_2}\left(j-m-1, \frac{2m-1-b_1+b_2}{2}\right) \\ + \tilde{\psi}_{0,b_2}\left(j-m-1, \frac{2m+1-b_1+b_2}{2}\right) \\ - \tilde{\psi}_{0,b_2+2}\left(j-m-1, \frac{2m+1-b_1+b_2}{2}\right) \\ + a\tilde{\psi}_{0,b_2+2}\left(j-m-1, \frac{2m+3-b_1+b_2}{2}\right) \end{aligned}$$

As $b_2 > 0$, we can use the relation given in (6.8) to find that

$$\Delta_{\mathcal{I}}\tilde{\psi}_{0,b_2+1}\left(j-m-1, \frac{2m+2-b_1+b_2}{2}\right) = 0.$$

Therefore, we have

$$T_a f_2(\mathtt{b},\mathtt{y}) = 0 \quad \mathtt{b} \in \mathcal{I}, \mathtt{y} \in \mathtt{B}_{AD}.$$

To summarize, we have

$$T_a C(\mathtt{b},\mathtt{y}) = \begin{cases} 1 & \text{if } \mathtt{b} = \mathtt{y} \\ 0 & \text{otherwise.} \end{cases}$$

6.2 The left hand boundary

Next, we check $T_a.C$ for $\mathtt{b}$ on the left hand boundary. For $\mathtt{b} \in \mathcal{L}$ we have that

$$T_a(\mathtt{b},\mathtt{w}) = \begin{cases} 1 & \text{if } \mathtt{w} = \mathtt{b} + e_1 \\ a\mathrm{i} & \text{if } \mathtt{w} = \mathtt{b} - e_2 \\ 0 & \text{otherwise.} \end{cases}$$

For $\mathtt{b} \in \mathcal{L}$ and $\mathtt{y} \in \mathtt{B}_{AD}$, using the above equation we find that (6.3) is given by

$$T_a f_i(\mathtt{b},\mathtt{y}) = f_i(\mathtt{b}+e_1,\mathtt{y}) + f_i(\mathtt{b}-e_2,\mathtt{y})a\mathrm{i} \tag{6.9}$$

Similar to the interior, we can expand $T_a f_1(\mathtt{b},\mathtt{w})$ in terms of $\tilde{\psi}$ and rewrite $T_a f_1(\mathtt{b},\mathtt{w})$ in terms of an integral using the definition of ψ given in (2.5). By a computation, we find that for $b_2 = y_2$, we obtain

$$\begin{aligned} T_a f_1(\mathtt{b},\mathtt{y}) &= \frac{1}{2\pi \mathrm{i}} \int_{\Gamma_{0,a}} \frac{e^{3\pi \mathrm{i} y_1/4} w^{-y_1/2}}{w-a} dw \\ &= \begin{cases} 1 & \text{if } y_1 = 0 \\ 0 & \text{otherwise.} \end{cases} \end{aligned} \tag{6.10}$$

because $y_1 \in 2\mathbb{N}$, as the integrand has no pole at infinity. For $b_2 > y_2$, we also find by computation that

$$\begin{aligned} T_a f_1(\mathtt{b},\mathtt{y}) = \frac{(-1)^{(-b_2+y_1-y_2)/4} \mathrm{i}^{y_1+y_2}}{2\pi \mathrm{i}} (1+a^2) \\ \times \int_{\Gamma_{0,a}} w^{-y_1/2} (w-a)^{(y_2-b_2-2)/2} (aw+1)^{(b_2-y_2-2)/2} dw \end{aligned}$$

As $b_2 > y_2$ (i.e. $b_2 \geq y_2 + 2$) and $y_1 \geq 0$, the integrand has no pole at infinity or $-1/a$, hence

$$T_a f_1(\mathtt{b},\mathtt{y}) = 0. \tag{6.11}$$

We find that for $b_2 < y_2$

$$T_a f_1(\mathtt{b},\mathtt{y}) = 0 \tag{6.12}$$

by using the same reasoning as the case for $\mathtt{b}$ in the interior, that is, each term in the expansion of $T_a f_1(\mathtt{b},\mathtt{y})$ in terms of $\tilde{\psi}$ is equal to zero.

Using Eqs. (6.10), (6.11) and (6.12) we have

$$T_a f_1(\mathtt{b},\mathtt{y}) = \begin{cases} 1 & \text{if } \mathtt{b} = \mathtt{y} \\ 0 & \text{otherwise} \end{cases} \tag{6.13}$$

for $\mathtt{b} \in \mathcal{L}$. Similar to the interior case, using the expansion of $T_a f_2(\mathtt{b},\mathtt{y})$ given in (6.9), we can expand using the definition of $f_2(\mathtt{b},\mathtt{w})$ to obtain

$$\begin{aligned} T_a f_2(\mathtt{b},\mathtt{y}) = (-1)^{(y_1-b_2-y_2)/4} \mathrm{i}^{y_1+y_2} \sum_{i,j=1}^{m} (A^{-1})_{i,j} \\ \times \tilde{\psi}_{1+y_2,2n+1}\left(\frac{2m+1-y_1+y_2}{2}, i-m-1\right) \\ \Delta_{\mathcal{L}} \tilde{\psi}_{0,b_2+1}\left(j-m-1, \frac{2m+2+b_2}{2}\right) \end{aligned} \tag{6.14}$$

where

$$\Delta_{\mathcal{L}}\tilde{\psi}_{0,b_2+1}\left(j-m-1,\frac{2m+2+b_2}{2}\right)=a\tilde{\psi}_{0,b_2}\left(j-m-1,\frac{2m-1+b_2}{2}\right)-\tilde{\psi}_{0,b_2+2}\left(j-m-1,\frac{2m+1+b_2}{2}\right).$$

We can rewrite the right hand side of the above equation in terms of its contour integral using (6.1) which gives

$$-\frac{1}{2\pi \mathrm{i}}\int_{\Gamma_{0,a}}(1+a^2)w^{-1+j-2m}(w-a)^{(-3-b_2)/2}(1+aw)^{(b_2-1)/2}dw.$$

Since $1\le j\le m, b_2\ge 1$ the integrand has no pole at $-1/a$ or infinity,hence the above quantity is zero and so the right hand side of (6.14) is equal to zero. Combining with (6.13) gives

$$T_aC(\mathtt{b},\mathtt{y})=\begin{cases}1 & \text{if } \mathtt{b}=\mathtt{y}\\ 0 & \text{otherwise}\end{cases}$$

for $\mathtt{b}\in\mathcal{L}$ and $\mathtt{y}\in \mathtt{B}_{AD}$.

6.3 The bottom boundary

We now consider the bottom boundary. We have that for $\mathtt{b}\in\mathcal{B}$

$$T_a(\mathtt{b},\mathtt{w})=\begin{cases}1 & \text{if } \mathtt{w}=\mathtt{b}+e_1\\ -a\mathrm{i} & \text{if } \mathtt{w}=\mathtt{b}+e_2\\ 0 & \text{otherwise.}\end{cases}$$

Using the above equation, (6.3) can be rewritten for $\mathtt{b}\in\mathcal{B}$ and is given by

$$T_af_i(\mathtt{b},\mathtt{y})=f_i(\mathtt{b}+e_1,\mathtt{y})-a\mathrm{i}f_i(\mathtt{b}+e_2,\mathtt{y}). \tag{6.15}$$

We first consider $T_af_1(\mathtt{b},\mathtt{w})$ for $b_2=y_2=-1$. Similar to the analogous computation for $\mathtt{b}$ in the interior, we can expand the right hand side of (6.15) in terms of ψ and rewrite the expression as an integral. By a computation, we find that

$$T_af_1(\mathtt{b},\mathtt{y})=\frac{(-1)^{(b_1+y_1)/4}\mathrm{i}^{y_1}}{2\pi\mathrm{i}}\int_{\Gamma_{0,a}}w^{(b_1-y_1-2)/2}dw$$
$$=\begin{cases}1 & \text{if } \mathtt{b}=\mathtt{y}\\ 0 & \text{otherwise.}\end{cases} \tag{6.16}$$

For $b_2 = -1 < y_2$, using the same reasoning as given for $\mathtt{b}$ in the interior, we have

$$T_a f_1(\mathtt{b}, \mathtt{y}) = 0. \tag{6.17}$$

Combining Eqs. (6.16) and (6.17), we have

$$T_a f_1(\mathtt{b}, \mathtt{y}) = \begin{cases} 1 & \text{if } b_1 = y_1 \\ 0 & \text{otherwise} \end{cases} \tag{6.18}$$

for $\mathtt{b} \in \mathcal{B}$ and $y \in \mathtt{B}_{AD}$. For $T_a f_2(\mathtt{b}, \mathtt{y})$, using (6.15) and following the same steps for the analogous computation for $\mathtt{b}$ in the interior, we have

$$\begin{aligned} T_a f_2(\mathtt{b}, \mathtt{y}) = (-1)^{(b_1 - b_2 + y_1 - y_2)/4} \mathrm{i}^{y_1 + y_2} \sum_{i,j=1}^{2m+1} (A^{-1})_{i,j} \\ \times \tilde{\psi}_{y_2+1, 2n+1}\left(\frac{2m+1-y_1+y_2}{2}, i-m-1\right) \\ \times \Delta_{\mathcal{B}} \tilde{\psi}_{0,2+b_2}\left(j-m-1, \frac{2m+2-b_1+b_2}{2}\right) \end{aligned}$$

where

$$\begin{aligned} &\Delta_{\mathcal{B}} \tilde{\psi}_{0,2+b_2}\left(j-m-1, \frac{2m+2-b_1+b_2}{2}\right) \\ &= -\tilde{\psi}_{0,b_2+2}\left(j-m-1, \frac{2m+1-b_1+b_2}{2}\right) \\ &\quad + a\tilde{\psi}_{0,b_2+2}\left(j-m-1, \frac{2m+3-b_1+b_2}{2}\right). \end{aligned}$$

We can rewrite the above equation using the integral definition of ψ. A computation gives

$$\Delta_{\mathcal{B}} \tilde{\psi}_{0,2+b_2}\left(j-m-1, \frac{2m+2-b_1+b_2}{2}\right) = \frac{-1}{2\pi \mathrm{i}} \int_{\Gamma_{0,a}} w^{-2+j-2m+b_1/2} dw = 0$$

because $b_1 \geq 4m+2$ by the co-ordinates of the bottom boundary. We have obtained

$$T_a f_2(\mathtt{b}, \mathtt{y}) = 0 \tag{6.19}$$

for $\mathtt{b} \in \mathcal{B}$ and $\mathtt{y} \in \mathtt{B}_{AD}$. Using (6.18) and (6.19) gives

$$T_a C(\mathtt{b}, \mathtt{y}) = \begin{cases} 1 & \text{if } \mathtt{b} = \mathtt{y} \\ 0 & \text{otherwise} \end{cases}$$

for $\mathtt{b} \in \mathcal{B}$ and $\mathtt{y} \in \mathtt{B}_{AD}$.

6.4 The top boundary

We can now consider $\mathtt{b} = (b_1, b_2)$ on the top boundary which means that $b_2 = 2n-1$ and $b_1 > 2n$. We have that for $\mathtt{b} \in \mathcal{T}$

$$T_a(\mathtt{b}, \mathtt{w}) = \begin{cases} -1 & \text{if } \mathtt{w} = \mathtt{b} - e_1 \\ a\mathrm{i} & \text{if } \mathtt{w} = \mathtt{b} - e_2 \\ 0 & \text{otherwise} \end{cases}$$

We can use the above equation to rewrite (6.3). We obtain for $\mathtt{b} \in \mathcal{T}$ and $y \in \mathtt{B}_{AD}$

$$T_a f_i(\mathtt{b}, \mathtt{y}) = -f_i(\mathtt{b} - e_1, \mathtt{y}) + a\mathrm{i} f_i(\mathtt{b} - e_2, \mathtt{y}) \tag{6.20}$$

We first consider $T_a f_1(\mathtt{b}, \mathtt{y})$ for $b_2 = y_2 = 2n-1$. By using the analogous expansion for $\mathtt{b}$ as the interior case in terms of ψ and its integral definition, we find that for $b_2 = y_2 = 2n-1$

$$T_a f_1(\mathtt{b}, \mathtt{y}) = 0. \tag{6.21}$$

For $y_2 < b_2 = 2n-1$, we find that

$$\begin{aligned} T_a f_1(\mathtt{b}, \mathtt{y}) = &-\frac{(-1)^{(1+b_1+y_1-y_2)/4}\mathrm{i}^{y_1+y_2-n}}{2\pi\mathrm{i}} \\ &\times \int_{\Gamma_{0,a}} \frac{\left(1-\frac{a}{w}\right)^{(1-2n+y_2)/2}(1+aw)^{(2n-1-y_2)/2}}{w^{(2n+1-b_1+y_1-y_2)/2}} dw. \end{aligned} \tag{6.22}$$

For $T_a f_2(\mathtt{b}, \mathtt{y})$, using (6.20) we can follow the analogous computation in the interior case, we find that

$$\begin{aligned} T_a f_2(\mathtt{b}, \mathtt{y}) = &(-1)^{(b_1-b_2+y_1-y_2)/4}\mathrm{i}^{y_1+y_2} \sum_{i,j=1}^{2m+1} (A^{-1})_{i,j} \\ &\times \tilde{\psi}_{y_2+1,2n+1}\left(\frac{2m+1-y_1+y_2}{2}, i-m-1\right) \\ &\times \Delta_{\mathcal{T}}\tilde{\psi}_{0,b_2}\left(j-m-1, \frac{2m-b_1+b_2}{2}\right) \end{aligned} \tag{6.23}$$

where

$$\begin{aligned} \Delta_{\mathcal{T}}\tilde{\psi}_{0,b_2}\left(j-m-1, \frac{2m-b_1+b_2}{2}\right) &= a\tilde{\psi}_{0,b_2}\left(j-m-1, \frac{2m-1-b_1+b_2}{2}\right) \\ &\quad + \tilde{\psi}_{0,b_2}\left(j-m-1, \frac{2m+1-b_1+b_2}{2}\right) \\ &= \frac{1}{2\pi\mathrm{i}} \int_{\Gamma_{0,a}} \frac{w^{-2+j-2m-n+b_1/2}(1+aw)^n}{\left(1-\frac{a}{w}\right)^n} dw \end{aligned}$$

which is found by expanding out the integrands using the integral definition of ψ given in (2.5) where we have used the fact that $b_2 = 2n - 1$. Notice that we can rewrite the right hand side of the above equation as

$$\begin{aligned}\frac{1}{2\pi \mathrm{i}} \int_{\Gamma_{0,a}} \frac{w^{-2+j-2m-n+b_1/2}(1+aw)^n}{\left(1-\frac{a}{w}\right)^n} dw \\ = \tilde{\psi}_{0,2n+1}\left(j-m-1, \frac{2m-b_1+2n}{2}\right) \\ - a\tilde{\psi}_{0,2n+1}\left(j-m-1, \frac{2m+2-b_1+2n}{2}\right). \end{aligned} \tag{6.24}$$

which follows by using expanding the right hand side of the above equation using the integral definition of ψ. By definition of the matrix A given in (6.2), we have

$$\sum_{j=1}^{m} (A^{-1})_{i,j} \tilde{\psi}_{0,2n+1}(j-m-1,k) = \delta_{i,k+m+1}. \tag{6.25}$$

Using (6.25) and (6.24) in (6.23) gives

$$\begin{aligned} T_a f_2(\mathtt{b},\mathtt{y}) &= (-1)^{(b_1-2n+1+y_1-y_2)/4} \mathrm{i}^{y_1+y_2} \\ &\times \left(\tilde{\psi}_{y_2+1,2n+1}\left(\frac{2m+1-y_1+y_2}{2}, \frac{2m-b_1+2n}{2}\right)\right. \\ &\left. - a\ \tilde{\psi}_{y_2+1,2n+1}\left(\frac{2m+1-y_1+y_2}{2}, \frac{2m+2-b_1+2n}{2}\right)\right) \\ &= \frac{(-1)^{(1+b_1+y_1-y_2)/4}\mathrm{i}^{y_1+y_2-n}}{2\pi \mathrm{i}} \int_{\Gamma_{0,a}} \frac{\left(1-\frac{a}{w}\right)^{(1-v2n+y_2)/2}(1+aw)^{(2n-1-y_2)/2}}{w^{(2n+1-b_1+y_1-y_2)/2}} dw \end{aligned} \tag{6.26}$$

Therefore, for $y_2 < b_2$ using (6.22) and (6.26) gives

$$T_a.(f_1+f_2)(\mathtt{b},\mathtt{y}) = 0. \tag{6.27}$$

For $y_2 = b_2 = 2n-1$, using (6.26) we have

$$T_a f_2(\mathtt{b},\mathtt{y}) = \frac{(-1)^{(b_1+y_1)/4}}{4} \mathrm{i}^{y_1} \int_{\Gamma_{0,a}} w^{(b_1-y_1-2)/2} dw = \begin{cases} 1 & \text{if } b_1 = y_1 \\ 0 & \text{otherwise.} \end{cases} \tag{6.28}$$

Finally, using (6.21), (6.27) and (6.28), we have

$$T_a C(\mathtt{b},\mathtt{y}) = \begin{cases} 1 & \text{if } b_1 = y_1 \\ 0 & \text{otherwise} \end{cases}$$

for $\mathtt{b} \in \mathcal{T}$ and $y \in \mathtt{B}_{AD}$.

6.5 The special point

Finally, we need to consider the special point, i.e. when we choose $\mathtt{b} = (2n, 2n-1)$. The special point has three neighboring white vertices and we have

$$T_a((2n,2n-1),\mathtt{w}) = \begin{cases} -1 & \text{if } \mathtt{w} = (2n-1, 2n-2) \\ -a\mathrm{i} & \text{if } \mathtt{w} = (2n-1, 2n) \\ a\mathrm{i} & \text{if } \mathtt{w} = (2n+1, 2n-2) \\ 0 & \text{otherwise} \end{cases}$$

For $\mathtt{b} = (2n, 2n-1)$ and $y \in \mathtt{B}_{AD}$, (6.3) becomes

$$T_a f_i(\mathtt{b}, \mathtt{y}) = -f_i(\mathtt{b} - e_1, y) + a\mathrm{i} f_i(\mathtt{b} - e_2, \mathtt{y}) - a\mathrm{i} f_i(\mathtt{b} + e_2, \mathtt{y}). \tag{6.29}$$

For $y_2 = 2n-1$, using the analogous steps for $\mathtt{b}$ in the interior, we can write using (6.29) and the integral definition of ψ

$$T_a f_1(\mathtt{b}, \mathtt{y}) = \frac{(-1)^{y_1/4}\mathrm{i}^{n+y_1}}{2\pi\mathrm{i}} \int_{\Gamma_{0,a}} \frac{a w^{(2n-1-y_1)/2}}{a-w} dw = 0, \tag{6.30}$$

since $y_1 \geq 2n+2$, when $y_2 = 2n-1$. For $y_2 < 2n-1$, we can write $T_a f_1(\mathtt{b}, \mathtt{w})$ using the integral definition of ψ given in (2.5). We obtain

$$\begin{aligned} T_a f_1(\mathtt{b}, \mathtt{y}) = &-\frac{(-1)^{(1+y_1-y_2)/4}\mathrm{i}^{y_1+y_2}}{2\pi\mathrm{i}} \\ &\times \int_{\Gamma_{0,a}} \frac{\left(1-\frac{a}{w}\right)^{(-1-2n+y_2)/2} (1+aw)^{(2n-1-y_2)/2}}{w^{(y_1+1-y_2)/2}} dw \end{aligned} \tag{6.31}$$

We can now expand out $T_a f_2(\mathtt{b}, \mathtt{y})$ using (6.29) and the analogous computations given in $\mathtt{b}$ in the interior. We find that

$$\begin{aligned} T_a f_2(\mathtt{b}, \mathtt{y}) = &(-1)^{(b_1-b_2+y_1-y_2)/4}\mathrm{i}^{y_1+y_2} \sum_{i,j=1}^{2m+1} (A^{-1})_{i,j} \\ &\times \tilde{\psi}_{1+y_2,2n+1}\left(\frac{2m+1-y_1+y_2}{2}, i-m-1\right) \\ &\times \Delta_{\mathcal{S}}\tilde{\psi}_{0,b_2}\left(j-m-1, \frac{2m-b_1+b_2}{2}\right) \end{aligned} \tag{6.32}$$

where

$$\begin{aligned} \Delta_{\mathcal{S}}\tilde{\psi}_{0,b_2}\left(j-m-1, \frac{2m-b_1+b_2}{2}\right) = &\, a\tilde{\psi}_{0,b_2}\left(j-m-1, \frac{2m-1-b_1+b_2}{2}\right) \\ &+\tilde{\psi}_{0,b_2}\left(j-m-1, \frac{2m+1-b_1+b_2}{2}\right) \\ &+a\tilde{\psi}_{0,b_2+2}\left(j-m-1, \frac{2m+3-b_1+b_2}{2}\right). \end{aligned}$$

By setting $\mathtt{b} = (2n, 2n-1)$, we have by a computation that

$$\Delta_{\mathcal{S}}\tilde{\psi}_{0,2n}\left(j-m-1, \frac{2m-2n+2n-1}{2}\right) = \frac{1}{2\pi \mathrm{i}} \int\limits_{\Gamma_{0,a}} \frac{w^{-2+j-2m}(1+aw)^n}{\left(1-\frac{a}{w}\right)^{n+1}} dw$$
$$= \tilde{\psi}_{0,2n+1}(j-m-1, m+1)$$

where the last equation follows from (2.5) and (6.1). We can substitute the above equation into (6.32) and use Eq. (6.25) in a similar way to the analogous computation found in the previous subsection. We find that

$$T_a f_2(\mathtt{b}, \mathtt{y}) = (-1)^{(b_1-b_2+y_1-y_2)/4} \mathrm{i}^{y_1+y_2} \tilde{\psi}_{1+y_2,2n+1}\left(\frac{2m+1-y_1+y_2}{2}, m+1\right)$$
$$= \frac{(-1)^{(1+y_1-y_2)/4} \mathrm{i}^{y_1+y_2}}{2\pi \mathrm{i}} \int\limits_{\Gamma_{0,a}} \frac{w^{(y_2-y_1-1)/2}(1+aw)^{(2n-1-y_2)/2}}{\left(1-\frac{a}{w}\right)^{(2n+1-y_2)/2}} dw \tag{6.33}$$

We have that for $y_2 = 2n-1$, (6.33) is equal to

$$T_a f_2(\mathtt{b}, \mathtt{y}) = \frac{1}{2\pi \mathrm{i}} \int\limits_{\Gamma_{0,a}} (-1)^{y_1/4} \mathrm{i}^{n+y_1} w^{n-1+y_1/2} dw = \begin{cases} 1 & \text{if } y_1 = 2n \\ 0 & \text{otherwise.} \end{cases}$$

for $\mathtt{b} = (2n, 2n-1)$.

Therefore, we have for $\mathtt{b} = (2n, 2n-1)$

$$T_a.C(\mathtt{b}, \mathtt{y}) = \sum_{i \in \{1,2\}} T_a f_i(\mathtt{b}, \mathtt{y}) = \begin{cases} 1 & \text{if } \mathtt{b} = \mathtt{y} \\ 0 & \text{otherwise} \end{cases}$$

by using Eqs. (6.30), (6.31) and (6.33) for $\mathtt{b} = (2n, 2n-1)$ and $y \in \mathtt{B}_{AD}$.

7 Proof of the formula for the $\mathbb{L}$-kernel

In this section, we derive the $\mathbb{L}$ kernel from the inverse Kasteleyn matrix. Let $b_j = (\xi_j, \eta_j)$, $1 \le j \le l$, be the positions of black vertices in Kasteleyn coordinates. We want to show that

$$\mathbb{P}\left[\mathbb{L}\text{-particles at } b_1, \ldots, b_l\right] = \det\left(\mathbb{L}_{n,\rho}\left(\xi_i, \eta_i; \xi_j, \eta_j\right)_{1 \le i,j, \le l}\right) \tag{7.1}$$

Note that we have an $\mathbb{L}$-particle at a black vertex of b if and only if a dimer (domino) covers the edges $(b, b+f_1)$ or $(b, b+f_2)$ where $f_1 = e_1$ and $f_2 = -e_2$. Hence, by Theorem 2.2 and the linearity of the determinant in its rows, we have that

$$\begin{aligned}
&\mathbb{P}\left[\mathbb{L}\text{-particles at } b_1, \dots, b_l\right] \\
&= \sum_{r_1,\dots,r_l}^{2} \prod_{j=1}^{l} K_a(b_i, b_i + f_{r_i}) \det\left(K_a^{-1}(b_i + f_{r_i}, b_j)\right)_{1\le i,j\le l} \\
&= \det\left(\sum_{r_i=1}^{2} K_a(b_i, b_i + f_{r_i}) K_a^{-1}(b_i + f_{r_i}, b_j)\right)_{1\le i,j\le l}
\end{aligned}$$

Recall that, from (2.6), we have that

$$K_a(b_i, b_i + f_1) = (-1)^{-(\xi_i+\eta_i+1)/2}$$

and

$$K_a(b_i, b_i + f_2) = (-1)^{-(\xi_i+\eta_i+1)/2} a\mathrm{i}.$$

If we use the formula (2.7) for the inverse Kasteleyn matrix, we see that

$$\begin{aligned}
&(-1)^{(\eta_2-\xi_2)/4-(\eta_1-\xi_1)/4} \sum_{r=1}^{2} K_a(b_1, b_1 + f_r) K_a^{-1}(b_1 + f_r, b_2) \\
&= \mathbb{K}_{n,\rho}\left(\eta_2 + 1, \frac{\eta_2 - \xi_2 + M}{2}; \eta_1 + 2, \frac{\eta_1 - \xi_1 + M}{2}\right) \\
&\quad - a\mathbb{K}_{n,\rho}\left(\eta_2 + 1, \frac{\eta_2 - \xi_2 + M}{2}; \eta_1, \frac{\eta_1 - \xi_1 + M - 2}{2}\right),
\end{aligned}$$

where $M = 2m + 1$ and we have used $(-1)^{-\eta_1} = -1$ since η_1 is odd. Thus, to prove (7.1) it suffices to show that

$$\begin{aligned}
\mathbb{L}_{n,\rho}(\xi_1, \eta_1; \xi_2, \eta_2) &= \mathbb{K}_{n,\rho}\left(\eta_2 + 1, \frac{\eta_2 - \xi_2 + M}{2}; \eta_1 + 2, \frac{\eta_1 - \xi_1 + M}{2}\right) \\
&\quad - a\mathbb{K}_{n,\rho}\left(\eta_2 + 1, \frac{\eta_2 - \xi_2 + M}{2}; \eta_1, \frac{\eta_1 - \xi_1 + M - 2}{2}\right)
\end{aligned}$$

Now, with $\varepsilon_i \in \{0, 1\}$ we have from (2.5) we have

$$\begin{aligned}
\mathbb{K}_{n,\rho}(2r + \varepsilon_1, x; 2s + \varepsilon_2, y) &= -\mathbb{I}_{2s+\varepsilon_2<2r+\varepsilon_1} \psi_{2r+\varepsilon_1,2s+\varepsilon_2}(x, y) \\
&\quad + (-1)^{x-y} S(2r + \varepsilon_1, x; 2s + \varepsilon_2, y) \\
&\quad - (-1)^{x-y} \left\langle ((\mathbb{I} - \mathbb{K})^{-1}_{2m+1} a_{-y,2s+\varepsilon_2})(k), b_{-x,2r+\varepsilon_1}(k) \right\rangle_{l^2(2m+1)} \\
&:= \sum_{i=0}^{2} R^{(i)}_{n,m}(2r + \varepsilon_1, x; 2s + \varepsilon_2, y).
\end{aligned}$$

Define

$$T^{(i)}_{n,m}(\xi_1,\eta_1;\xi_2,\eta_2) = R^{(i)}_{n,m}\left(\eta_2+1,\frac{\eta_2-\xi_2+M}{2};\eta_1+2,\frac{\eta_1-\xi_1+M}{2}\right) - aR^{(i)}_{n,m}\left(\eta_2+1,\frac{\eta_2-\xi_2+M}{2};\eta_1,\frac{\eta_1-\xi_1+M-2}{2}\right). \quad (7.2)$$

We have to show that

$$\sum_{i=0}^{2} T^{(i)}_{n,m}(2r+\varepsilon_1,x;2s+\varepsilon_2,y) = \mathbb{L}_{n,\rho}(\xi_1,\eta_1;\xi_2,\eta_2). \quad (7.3)$$

Since η_1 and η_2 are odd we can write $\eta_1 = 2s-1$, $\eta_2 = 2r-1$ so that $\eta_2+1 = 2r$ and $\eta_1 = 2(s-1)+1$ and $\eta_1+2 = 2s+1$. Now by (2.5),

$$\begin{aligned} &T^{(0)}_{n,m}(\xi_1,\eta_1;\xi_2,\eta_2) \\ &= -\frac{\mathbb{I}_{2s+1<2r}}{2\pi i}\int_{\Gamma_{0,a}} \frac{(1+az)^{s-r}}{(1-a/z)^{s-r+1}} z^{(\eta_2-\eta_1)/2+(\xi_1-\xi_2)/2}\frac{dz}{z} \\ &\quad + \frac{a\mathbb{I}_{2s-1<2r}}{2\pi i}\int_{\Gamma_{0,a}} \frac{(1+az)^{s-1-r}}{(1-a/z)^{s-r}} z^{(\eta_2-\eta_1)/2+(\xi_1-\xi_2)/2+1}\frac{dz}{z}. \end{aligned} \quad (7.4)$$

If $\eta_1 > \eta_2$, i.e. $s \geq r+1$, then $2s+1 > 2s-1 > 2r$ and the expression in the right hand side of (7.4) is equal to zero. If $\eta_1 = \eta_2$, i.e. $r = s$, we get

$$\begin{aligned} &\frac{a}{2\pi i}\int_{\Gamma_{0,a}} \frac{z^{(\xi_1-\xi_2)/2}}{1+az}dz = \frac{a\mathbb{I}_{\xi_1<\xi_2}}{2\pi i}\int_{\Gamma_{0,a}} \frac{z^{(\xi_1-\xi_2)/2}}{1+az}dz \\ &= -\frac{\mathbb{I}_{\xi_1<\xi_2}}{2\pi i}\int_{\Gamma_{-1/a}} \frac{z^{(\xi_1-\xi_2)/2}}{z+1/a}dz = -\mathbb{I}_{\xi_1<\xi_2}\left(-\frac{1}{a}\right)^{(\xi_1-\xi_2)/2}. \end{aligned}$$

because of the change of orientation from moving the contour $\Gamma_{0,a}$ to the contour $\Gamma_{-1/a}$. Thus,

$$\begin{aligned} T^{(0)}_{n,m}(\xi,\eta_1;\eta_2,\xi_2) &= -\mathbb{I}_{\eta_1<\eta_2}\frac{1+a^2}{2\pi i}\int_{\Gamma_{0,a}} \frac{(1+az)^{(\eta_1-\eta_2)/2-1}}{(z-a)^{(\eta_1-\eta_2)/2+1}} z^{(\xi_1-\xi_2)/2}dz \\ &\quad -\mathbb{I}_{\xi_1<\xi_2}\mathbb{I}_{\eta_1=\eta_2}(-a)^{(\xi_2-\xi_1)/2}. \end{aligned} \quad (7.5)$$

If $\xi_1 \geq \xi_2$ and $\eta_1 < \eta_2$ the integral in (7.5) is equal to 0 since the integrand is analytic inside $\Gamma_{0,a}$. Thus, the first term in (7.5) equals

$$-\mathbb{I}_{\eta_1<\eta_2}\mathbb{I}_{\xi_1<\xi_2}\frac{1+a^2}{2\pi i}\int_{\Gamma_{0,a}}\frac{(1+az)^{(\eta_1-\eta_2)/2-1}}{(z-a)^{(\eta_1-\eta_2)/2+1}}z^{(\xi_1-\xi_2)/2}dz$$
$$=-(1-\mathbb{I}_{\eta_1>\eta_2}-\mathbb{I}_{\eta_1=\eta_2})\mathbb{I}_{\xi_1<\xi_2}\frac{1+a^2}{2\pi i}\int_{\Gamma_{0,a}}\frac{(1+az)^{(\eta_1-\eta_2)/2-1}}{(z-a)^{(\eta_1-\eta_2)/2+1}}z^{(\xi_1-\xi_2)/2}dz.$$

The last integral is equal to zero if $\eta_1 > \eta_2$ and hence the last expression equals

$$-\mathbb{I}_{\eta_1=\eta_2}\mathbb{I}_{\xi_1<\xi_2}\frac{1+a^2}{2\pi i}\int_{\Gamma_{-1/a}}\frac{z^{(\xi_1-\xi_2)/2}}{(1+az)(z-a)}dz$$
$$-\mathbb{I}_{\xi_1<\xi_2}\frac{1+a^2}{2\pi i}\int_{\Gamma_{0,a}}\frac{(1+az)^{(\eta_1-\eta_2)/2-1}}{(z-a)^{(\eta_1-\eta_2)/2+1}}z^{(\xi_1-\xi_2)/2}dz.$$

The first term in this expression equals

$$\mathbb{I}_{\eta_1=\eta_2}\mathbb{I}_{\xi_1<\xi_2}\left(-\frac{1}{a}\right)^{(\xi_1-\xi_2)/2}$$

so combining this result with (7.5) we find

$$T^{(0)}_{n,m}(\xi_1,\eta_1;\xi_2,\eta_2)$$
$$=-\mathbb{I}_{\xi_1<\xi_2}\frac{1+a^2}{2\pi i}\int_{\Gamma_{0,a}}\frac{(1+az)^{(\eta_1-\eta_2)/2-1}}{(z-a)^{(\eta_1-\eta_2)/2+1}}z^{(\xi_1-\xi_2)/2}. \tag{7.6}$$

Next, using (2.5) and inserting it into (7.2) we get

$$T^{(1)}_{n,m}(\xi_1,\eta_1;\xi_2,\eta_2)$$
$$=\frac{1+a^2}{(2\pi i)^2}\int_{\Gamma_{0,a}}dv\int_{\Gamma_{0,a,v}}\frac{dv}{v-u}\frac{v^{n-\xi_2/2}}{u^{n-\xi_1/2}}\frac{(1+au)^{(\eta_1-1)/2}(u-a)^{n-(\eta_1+1)/2}}{(1+av)^{(\eta_2+1)/2}(v-a)^{n-(\eta_2-1)/2}} \tag{7.7}$$

after a short computation. Finally, by (7.2) and (2.5) we see that

$$T^{(2)}_{n,m}(\xi_1,\eta_1;\xi_2,\eta_2)$$
$$=\langle(\mathbb{I}-K)^{-1}_{2m+1}(a_{-(\eta_1-\xi_1+M)/2,2s+1}+aa_{-(\eta_1-\xi_1+M-2)/2,2s-1})(k),$$
$$b_{-(\eta_2-\xi_2+M)/2,2r}(k)\rangle_{\geq 2m+1}(-1)^{(\eta_2-\xi_2+M)/2-(\eta_1-\xi_1+M-2)/2}.$$

Now, using (2.5) a computation gives

$$(-1)^{-(\eta_1-\xi_1+M-2)/2}\left(a_{-(\eta_1-\xi_1+M)/2,2s+1}(k)+aa_{-(\eta_1-\xi_1+M-2)/2,2s-1}(k)\right)$$
$$=\frac{(-1)^k(1+a^2)}{(2\pi i)^2}\int_{\Gamma_{0,a}}du\int_{\Gamma_{0,a,u}}\frac{dv}{u-v}\frac{v^{(\xi_1-\eta_1-1)/2}}{u^{k+1}}$$

$$\times \frac{(1+av)^{(\eta_1-1)/2}(1-a/v)^{n-(\eta_1+1)/2}}{(1+av)^n(v-a)^{n+1}}$$
$$= -(1+a^2)A_{\xi_1,\eta_1}(k). \tag{7.8}$$

Note that by moving the v-contour in (7.8) inside the u-contour we get the expression in (2.2). Similarly, by (2.5),

$$b_{-(\eta_2-\xi_2+M)/2,2r}(k)(-1)^{(\eta_2-\xi_2+M)/2}$$
$$= \frac{(-1)^k}{(2\pi i)^2}\int_{\Gamma_{0,a}} du \int_{\Gamma_{0,a,u}} \frac{dv}{v-u}\frac{v^k}{u^{(\xi_2-\eta_2+1)/2}}\frac{(1+av)^n(w-a)^{n+1}}{(1+av)^{(\eta_2+1)/2}(1-a/v)^{n-(\eta_2-1)/2}}$$
$$= B_{\xi_2,\eta_2}(k)$$

Again by moving the v-contour inside the u-contour we get the expression in (2.2). Thus,

$$T^{(2)}_{n,m}(\xi_1,\eta_1;\xi_2,\eta_2) = -\left\langle ((\mathbb{I}-K)^{-1}_{2m+1}A_{\xi_1,\eta_1})(k), B_{\xi_2,\eta_2}(k)\right\rangle_{\geq 2m+1}(1+a^2). \tag{7.9}$$

If we use (7.6), (7.7) and (7.9) we obtain (7.3) which is what we wanted to prove.

References

1. Adler, M., Ferrari, P.L., van Moerbeke, P.: Nonintersecting random walks in the neighborhood of a symmetric tacnode. Ann. Prob. **41**(4), 2599–2647 (2013)
2. Adler, M., Johansson, K., van Moerbeke, P.: Double Aztec diamonds and the tacnode process. Adv. Math. **252**, 518–571 (2014)
3. Adler, M., van Moerbeke, P.: Coupled GUE-minor processes. arXiv:1312.3859 (2013)
4. Borodin, A., Ferrari, P.L.: Anisotropic growth of random surfaces in 2 + 1 dimensions. Commun. Math. Phys. **325**(2), 603–684 (2014)
5. Chhita, S., Johansson, K., Young, B.: Asymptotic domino statistics in the Aztec diamond. arXiv:1212.5414 (2012)
6. Cohn, H., Kenyon, R., Propp, J.: A variational principle for domino tilings. J. Am. Math. Soc. **14**(2), 297–346 (electronic) (2001)
7. Delvaux, S.: The tacnode kernel: equality of Riemann-Hilbert and Airy resolvent formulas. arXiv:1211.4845 (2012)
8. Elkies, N., Kuperberg, G., Larsen, M., Propp, J.: Alternating-sign matrices and domino tilings I. J. Algebraic Combin. **1**(2), 111–132 (1992)
9. Elkies, N., Kuperberg, G., Larsen, M., Propp, J.: Alternating-sign matrices and domino tilings II. J. Algebraic Combin. **1**(3), 219–234 (1992)
10. Ferrari, P.L., Spohn, H.: Step fluctuations for a faceted crystal. J. Stat. Phys. **113**(1–2), 1–46 (2003)
11. Ferrari, P.L., Vető, B.: Non-colliding Brownian bridges and the asymmetric tacnode process. Electron. J. Probab. **17**(44), 17 (2012)
12. Helfgott, H.: Edge effects on local statistcs in lattice dimers: a study of the Aztec diamond (finite case). arXiv:0007:7136 (2000)
13. Jockusch, W., Propp, J., Shor, P.: Random domino tilings and the Arctic Circle Theorem. arXiv.org/abs/math.CO/9801068 (1998)
14. Johansson, K.: Non-intersecting paths, random tilings and random matrices. Prob. Theory Relat. Fields **123**(2), 225–280 (2002)
15. Johansson, K.: The arctic circle boundary and the Airy process. Ann. Prob. **33**(1), 1–30 (2005)

16. Johansson, K.: Non-colliding Brownian motions and the extended tacnode process. Commun. Math. Phys. **319**(1), 231–267 (2013)
17. Johansson, K., Nordenstam, E.: Eigenvalues of GUE minors. Electron. J. Prob. **11**(50), 1342–1371 (2006)
18. Kasteleyn, P.W.: The statistics of dimers on a lattice: I. The number of dimer arrangements on a quadratic lattice. Physica **27**, 1209–1225 (1961)
19. Kenyon, R.: Local statistics of lattice dimers. Ann. Inst. H. Poincaré Prob. Stat. **33**(5), 591–618 (1997)
20. Luby, M., Randall, D., Sinclair, A.: Markov chain algorithms for planar lattice structures. SIAM J. Comput. **31**(1), 167–192 (2001)
21. Okounkov, A., Reshetikhin N.: Correlation function of Schur process with application to local geometry of a random 3-dimensional Young diagram. J. Am. Math. Soc. **16**(3), 581–603 (electronic) (2003)
22. Propp, J.: Generalized domino-shuffling. Theor. Comput. Sci. **303**(2–3), 267–301 (2003) (Tilings of the plane)
23. Romik, D.: Arctic circles, domino tilings and square Young tableaux. Ann. Prob. **40**(2), 611–647 (2012)